



**HAL**  
open science

## Rapport sur le suivi morphosédimentaire du sillon de Talbert pour l'année 2017

Pierre Stéphan, Bernard Fichaut, Serge S. Suanez, Ronan Autret, Julien  
Houren

► **To cite this version:**

Pierre Stéphan, Bernard Fichaut, Serge S. Suanez, Ronan Autret, Julien Houren. Rapport sur le suivi morphosédimentaire du sillon de Talbert pour l'année 2017. [Rapport de recherche] LETG-Brest UMR 6554 CNRS; Université de Bretagne Occidentale (UBO). 2018. hal-01730956

**HAL Id: hal-01730956**

**<https://hal.science/hal-01730956>**

Submitted on 13 Mar 2018

**HAL** is a multi-disciplinary open access archive for the deposit and dissemination of scientific research documents, whether they are published or not. The documents may come from teaching and research institutions in France or abroad, or from public or private research centers.

L'archive ouverte pluridisciplinaire **HAL**, est destinée au dépôt et à la diffusion de documents scientifiques de niveau recherche, publiés ou non, émanant des établissements d'enseignement et de recherche français ou étrangers, des laboratoires publics ou privés.



ueb  
U  
B  
O

université  
de bretagne  
occidentale

Pierre STÉPHAN  
Bernard FICHAUT  
Serge SUANEZ  
Ronan AUTRET  
Julien HOURON

# Rapport sur le suivi morphosédi- mentaire du sillon de Talbert pour l'année 2017

Mars 2018



INSTITUT  
UNIVERSITAIRE  
EUROPÉEN  
DE LA MER



***Suivi morphosédimentaire du Sillon de Talbert pour l'année 2017***  
***(Commune de Pleubian – Période d'octobre 2016 à septembre 2017)***

***Pierre STÉPHAN***  
***Bernard FICHAUT***  
***Serge SUANEZ***  
***Ronan AUTRET***  
***Julien HOURON***

## COMMUNE DE PLEUBIAN (CÔTES D'ARMOR) ET CONSERVATOIRE DE L'ESPACE LITTORAL ET DES RIVAGES LACUSTRES



### ***Suivi morphosédimentaire du Sillon de Talbert pour l'année 2017 (Commune de Pleubian – Période d'octobre 2016 à septembre 2017)***



#### **Maître d'œuvre**

GEOMER - UMR 6554 CNRS - Institut Universitaire Européen de la Mer - Place Nicolas Copernic, 29280 Plouzané

*Réalisation : Pierre STÉPHAN, Bernard FICHAUT, Serge SUANEZ, Ronan AUTRET, Julien HOURON*  
pierre.stephan@univ-brest.fr; bernard.fichaut@univ-brest.fr ; serge.suanez@univ-brest.fr

*Direction scientifique : Pierre Stéphan, Serge Suanez et Bernard Fichaut*  
pierre.stephan@univ-brest.fr ; serge.suanez@univ-brest.fr ; bernard.fichaut@univ-brest.fr

## 1-Introduction

La présente étude s'inscrit dans la continuité du suivi topo-morphologique du Sillon de Talbert initié en 2003 à la demande de la commune de Pleubian et du Conservatoire du Littoral. L'objectif est d'analyser les modalités d'évolution de la flèche depuis l'enlèvement de l'enrochement en 2004 (Stéphan et al., 2007, 2008, 2009, 2011, 2012, 2015 ; Fichaut et al., 2010, 2013). Dans le cadre de ce rapport, nous présentons les principaux changements morphologiques survenus entre les levés topographiques effectués aux mois d'octobre 2016 et septembre 2017 à l'échelle du Sillon.

La méthode que nous avons employée pour reconstituer la topographie de l'estran respecte en partie le protocole de mesure détaillé dans nos précédents rapports. Elle s'appuie sur l'acquisition de mesures topographiques au DGPS (type TopCon HiperV) à partir d'une station fixe installée sur la borne IGN située sur le sémaphore de Créac'h Maout, dont les coordonnées géodésiques sont accessibles sur le site de l'IGN ([www.ign.fr/](http://www.ign.fr/) rubrique Géodésie). Notons qu'en 2016, nous avons réalisé nos mesures à partir d'une méthode impliquant le survol du Sillon au drone et l'acquisition d'images aériennes. Cette technique n'a pas été employée en 2017 pour des raisons que nous expliquerons dans la section 2 de ce rapport.

Enfin, un travail important a été réalisé au cours de l'année 2017 à travers la rédaction d'un article scientifique soumis à la revue Ocean & Coastal Management. Dans cette publication, nous avons approfondi l'analyse morphologique du Sillon de Talbert sur la période 2002-2017. Une synthèse des bilans sédimentaires a été réalisée. Un travail plus fin a également été mené sur le secteur de la taille de guêpe en voie de rupture. Des propositions concrètes en vue d'un éventuel rechargement sédimentaire de ce secteur ont été formulées. Cet article figure en annexe de ce rapport.

## 2-Méthodologie des relevés

### 2.1- Source des données utilisées pour le relevé de septembre 2017

Trois semis de points topographiques ont été utilisés pour produire le Modèle Numérique de Terrain de septembre 2017 (fig. 1) :

1- un semis de points « invariables » relevés au DGPS lors des précédentes campagnes de mesures et que nous avons réutilisé dans les secteurs qui n'ont pas enregistré de changements morphologiques perceptibles ;

2- un semis de points relevés au mois de septembre 2017 à l'aide d'un DGPS sur les secteurs mobiles du sillon que nous détaillons dans le point 2.2.

3- un semis de points « invariables » qui couvre les estrans et zones terrestres environnants le Sillon a été ajouté pour améliorer les aspects de visualisation du MNT. Ce semis de point est issu d'un relevé LIDAR réalisé en octobre 2002.

La topographie a été modélisée sous le logiciel Surfer 10 en utilisant le krigeage comme modèle d'interpolation avec intégration des lignes de rupture de pente. La topographie du mois de septembre 2017 (fig.2A) a ensuite été comparée à celle d'octobre 2016 afin d'effectuer le bilan morpho-sédimentaire de l'année (fig.2B).

### 2.2. Les relevés au DGPS

Les relevés au DGPS (modèle TopCon Hyper-V) ont été réalisés du 04 au 07 septembre 2017 à partir d'une station fixe et de 4 mobiles fonctionnant simultanément. Un total de 14773 points de mesure ont été relevés sur le terrain de cette façon (fig. 1). 220 lignes de rupture de pente ont également été relevées sur le terrain afin d'être intégrées aux modélisations numériques. Un ensemble de 2307 points « invariables » relevés au cours des précédentes années au DGPS ont été ajoutés, ainsi que 67 lignes de ruptures de pente « fixes ».

### 2.3-Pourquoi avoir abandonné les survols au drone en 2017 ?

Les relevés des mois d'avril et d'octobre 2016 ont été effectués à partir d'une nouvelle technique basée sur l'utilisation de photographies stéréoscopiques. Ce protocole avait été mis en œuvre afin d'améliorer la qualité de la mesure topo-morphologique. La méthode reposait sur l'utilisation d'un drone exocoptère autopiloté. Equipé d'un appareil photo reflex Nikon D800, les survols du sillon avaient permis l'acquisition d'images à une altitude moyenne de 115 m. A partir de ces prises de vue, la topographie du Sillon avait été reconstituée selon le principe de la stéréophotogrammétrie sous le logiciel Agisoft PhotoScan afin de générer un nuage de points topographiques de très forte densité. Cette méthode avait permis de produire deux principales données : (i) une orthophotographie de la zone survolée et (ii) un nuage de points de très forte densité comptant 56 812 000 de points, soit 146 points en moyenne par m<sup>2</sup>. En définitive, le Modèle Numérique de Terrain réalisé présentait une très haute résolution (10x10 cm).

Comme nous l'avons indiqué dans un précédent rapport d'étude (Stéphan et al., 2016 ; Fichaut et al., 2017), les données issues des survols au drone peuvent présenter des erreurs significatives par endroits, en particulier si le recoupement entre les prises de vues aériennes n'est pas suffisant. Le logiciel manque alors d'informations pour restituer la topographie et génère des données aberrantes, en particulier en terme d'altitude. C'est le constat que nous avons pu tirer du relevé effectué en avril 2016. Conscient de ce problème, le relevé suivant (octobre 2016) a été mené en veillant scrupuleusement au bon recouvrement des clichés (Fichaut et al., 2017). Mais en dépit de ces précautions, une incertitude d'environ +/- 15 cm en z a été estimée sur le MNT. De plus, nous avons constaté que cette erreur n'était pas répartie de façon

homogène sur l'ensemble de la zone d'étude. Ainsi, la partie médiane présentait localement une incertitude importante.

L'origine de cette erreur est difficile à déterminer. Le logiciel de traitement que nous utilisons (Agisoft PhotoScan) est une « boîte noire » qui ne permet pas de contrôler et corriger les différents paramètres de calcul. La morphologie particulière du Sillon, en particulier dans sa partie médiane, caractérisée par de très fortes pentes et peu d'éléments visuels remarquables (absence de végétation, de rochers), pourrait expliquer que le logiciel de calcul ne soit pas en mesure de reconstituer précisément la topographie par stéréo-photogrammétrie. Des relevés similaires effectués sur des plages moins étendues donnent de meilleurs résultats. La taille de la zone d'étude et la quantité des données à traiter pourrait donc constituer une limite supplémentaire.

Or, dans le cadre de suivis topo-morphologiques, il est important de minimiser les erreurs de positionnement altitudinal des mesures (Suanez et al., 2008) car celles-ci se reportent sur tous les calculs volumiques. Ainsi, concernant aux bilans sédimentaires calculés entre octobre 2016 et septembre 2017 sur le Sillon de Talbert, nous avons dû considérer une « marge d'erreur moyenne » de +/- 20 cm en z. Cela signifie que les changements de la topographie inférieurs à 20 cm n'ont pas été considérés comme significatifs. Cette incertitude se reporte aussi sur les calculs volumiques que nous avons réalisés entre octobre 2016 et septembre 2017. L'incertitude est telle que la plupart des bilans volumiques obtenus ne peuvent être considérés comme significatifs. Ils sont donc à considérer uniquement comme des ordres de grandeur.

### 3- Evolutions morphologiques entre octobre 2016 et septembre 2017

D'une façon générale, les changements morphologiques mesurés sur le Sillon de Talbert entre octobre 2016 et septembre 2017 traduisent une évolution en deux temps. Une première phase, probablement durant l'hiver, a causé un franchissement de la crête par de fortes vagues et, par endroit, un déversement des sédiments sur le revers. Cette érosion s'est manifestée lors d'un ou plusieurs épisodes de pleines mers de vive-eau. Là où la crête n'a pas été franchie, elle a néanmoins subi une érosion. L'ampleur de cette érosion est restée relativement modeste, et sans commune mesure avec les épisodes morphogènes de l'hiver 2013-2014 ou de février 2016 (tempête Imogen). Ainsi, le Sillon n'a pas subi d'écroulement spectaculaire. Les volumes qui ont été érodés sur la plage et déversés sur le revers sont restés faibles. Une seconde phase est venue partiellement gommer la signature érosive de l'hiver et s'est traduit par un redressement du profil du cordon, par la formation localisée d'une berme et, dans quelques secteurs spécifiques, par l'accumulation de matériel au sommet du cordon où la crête a connu un exhaussement.

Les principales modifications morphologiques sont synthétisées dans la figure 3 et sont décrites comme suit :

#### (1, fig. 3) : la plage du Chouck

Entre octobre 2016 et septembre 2017, les évolutions morphologiques ont été de faibles ampleurs le long de la plage du Chouck. En dépit des grandes incertitudes qui entachent le calcul des volumes sédimentaires, on peut considérer que le bilan est resté stable sur toute la période. Une érosion est enregistrée sur le haut de plage, au pied de l'enrochement et au pied de la dune, probablement lors d'une période tempétueuse ou d'un événement de tempête assez énergétique. Par la suite, une tendance au redressement du profil de la plage a conduit à une remontée des sables depuis le bas vers le haut de plage où une berme s'est formée au niveau des PMVE.

#### (2, fig. 3) : la partie proximale

Dans sa partie proximale, le Sillon a enregistré de très faibles évolutions morphologiques. Dans l'ensemble, la crête s'est surélevée de quelques centimètres seulement. Quelques points d'érosion, très localisés, ont été mesurés au sommet du cordon où la dune embryonnaire a été érodée (au niveau du profil P035). Le bas de plage a également perdu des sédiments au profit du sommet du cordon où une berme s'est constituée au niveau des PMVE (vers le profil P050). A ce niveau, la crête a enregistré un exhaussement de 30 cm en moyenne (fig. 4).

#### (3, fig. 3) : la partie médiane

Au sommet du cordon, les vagues de tempêtes hivernales ont creusé des petits couloirs où se sont concentrés les flux de sédiments franchissant la crête. A ce niveau, l'altitude de la crête s'est abaissée de 15 à 35 cm (fig. 4). Au droit de ces couloirs, le matériel s'est accumulé sur le revers et le cordon a reculé de 10 m par endroits. La zone la plus touchée par les franchissements est située entre les profils P050 et P060 où le recul du cordon est estimé à -2,5 m en moyenne. Entre les profils P065 et P090, le recul du cordon est moindre, de -0,6 m en moyenne. Suite à cet épisode de franchissement, une tendance au redressement du cordon a permis un exhaussement de la crête d'une vingtaine de cm en moyenne et la formation d'une berme au niveau des PMVE. Le long de la plage, un volume sédimentaire d'environ 1000 m<sup>3</sup> a été déplacé vers la pointe.

#### (4, fig. 3) : la partie distale et le lobe de jusant

Les principaux changements morphologiques mesurés dans la partie distale sont le fait des déplacements de galets vers la pointe nord-est du Sillon où un volume d'environ 1200 m<sup>3</sup> s'est accumulé entre les mois d'octobre 2016 et de septembre 2017. Le lobe de jusant, soumis aux actions conjuguées de la houle et de la marée, a adopté une morphologie bi-lobée qui traduit un déplacement du matériel en deux temps : (T1, fig.) un mouvement préférentiel vers l'est, sous l'action des houles hivernales, puis (T2, fig.) une prédominance des courants de jusant qui redistribuent les sédiments vers l'ouest.

#### (5, fig. 3) : le revers de la spatule

Les bilans volumiques calculés sur la période indiquent une érosion importante à l'extrémité nord-est du revers de la spatule. Environ 3000 m<sup>3</sup> de galets ont été érodés dans ce secteur. Compte tenu de l'incertitude des données, il nous est difficile de déterminer précisément les secteurs où ce matériel s'est accumulé. Comme nous

l'avons rappelé plus haut, les cartes présentées dans la figure tiennent compte uniquement des variations topographiques supérieures à 20 cm. Il est donc probable que ces volumes aient été redistribués sur l'ensemble du revers de la spatule sans que nous puissions l'observer. En revanche, nous pouvons affirmer qu'une partie de ce matériel (environ 1000 m<sup>3</sup>) a été transporté jusqu'au sommet du cordon pour édifier une nouvelle crête d'accrétion. Sur le revers de la partie médiane, des sinuosités se sont également accentuées et reflètent un transit des galets vers le sud-ouest par les houles secondaires.

### (6, fig. 3) : le contact avec l'île Blanche

Le point de contact entre le Sillon et l'île blanche constitue une zone de fragilité potentielle (Fichaut et al., 2017). En octobre 2017, quelques mètres seulement séparent les deux cordons. Le chenal de marée qui serpente dans ce goulet d'étranglement est emprunté par des courants particulièrement forts. Entre les mois d'octobre 2016 et de septembre 2017, ces courants ont provoqué le sapement du revers du Sillon. Cela explique qu'une « avancée » relative de 2,2 m a été mesurée au niveau du profil P062.

### (7, fig. 3) : l'ensablement des ados

Depuis plusieurs années, les ados artificiels situés en arrière du Sillon tendent à être recouverts par les sédiments sableux qui s'accumulent sur le revers. Cet ensablement se traduit par la formation de lobes sableux qui s'étalent vers l'est. Entre les profils P020 et P040, ces lobes se sont étalés sur une dizaine de mètres par endroits durant la période d'étude.

## 4- Bilan du suivi topo-morphologique à haute fréquence du sillon de Talbert le long de deux profils de mesure

### 4.1 - Rappel de la méthode et des objectifs du suivi à haute fréquence

Depuis le mois de septembre 2012, un suivi morphologique et hydrodynamique à haute fréquence a été mis en place en parallèle du suivi topo-morphologique annuel de l'ensemble du sillon (effectué quant à lui depuis 2006). Nous ne décrivons pas les aspects méthodologiques de ce suivi qui ont déjà été largement détaillés dans les rapports annuels de 2012 et 2013 (Stéphan et al., 2012 ; Fichaut et al., 2013) ; nous rappellerons simplement que ce travail d'observation repose (i) sur des levés topographiques mensuels réalisés le long de deux profils localisés dans les parties les plus mobiles du sillon, (ii) et sur des mesures de houles et de hauteurs d'eau effectuées à partir d'un capteur de pression installé au niveau du profil B (figure A).

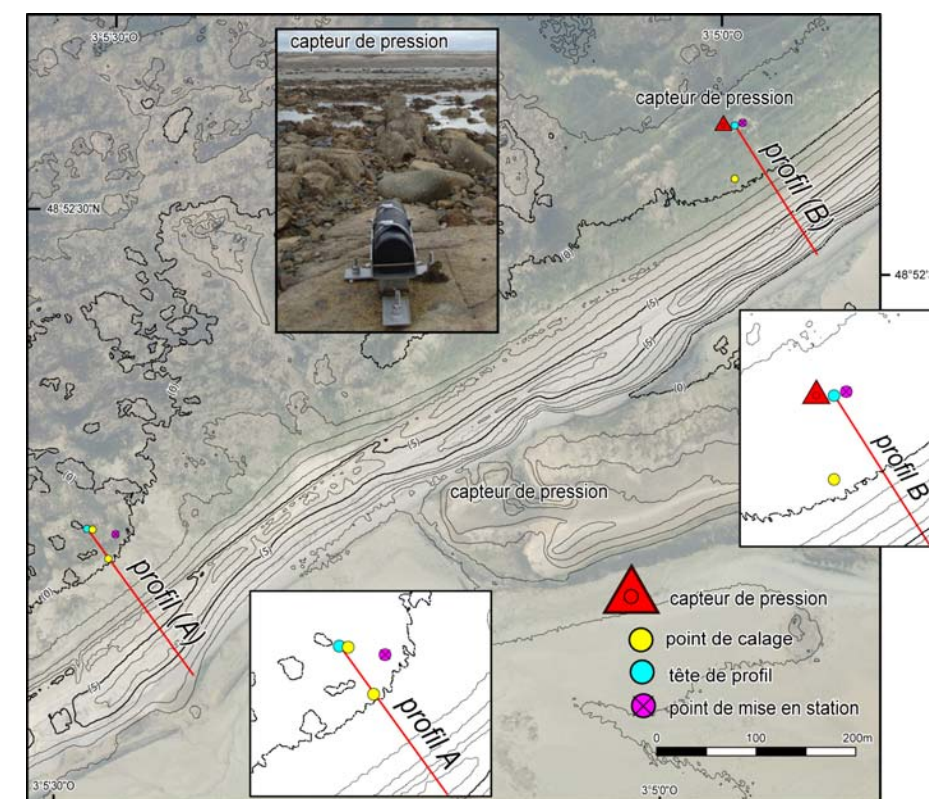


Figure A – localisation des deux profils de mesures topo-morphologiques et du capteur de pression de houle et de niveaux d'eau.

L'objectif de ce suivi à haute fréquence est de mesurer et de quantifier l'impact de tous les épisodes tempétueux agissant à une échelle épisodique et/ou d'évaluer les processus de régénération (en période de temps calme) agissant là encore à des échelles courtes (mensuelles). Ainsi, entre les mois de septembre 2012 et de janvier 2018, 97 profils de plage ont été levés le long des deux profils A et B (figure B).

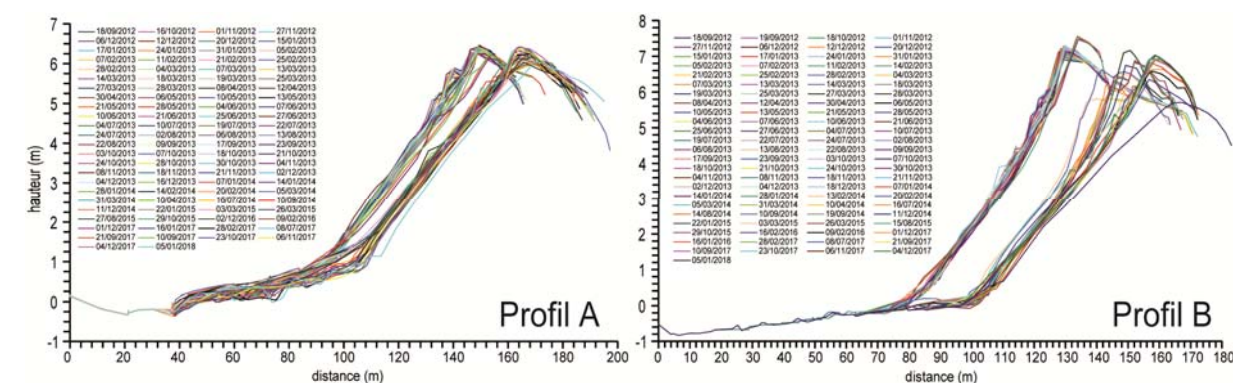


Figure B - Enveloppe de profils topo-morphologiques A et B entre les mois de septembre 2012 et de janvier 2018.

Le dernier bilan effectué sur ces mesures datait du mois de décembre 2014 (Fichaut et al., 2015), et faisait suite à la série de tempêtes de l'hiver 2013-2014. Ces levés avaient permis d'évaluer pertinemment à plus de -20 m le recul du sillon de Talbert au niveau des deux profils (figure C).

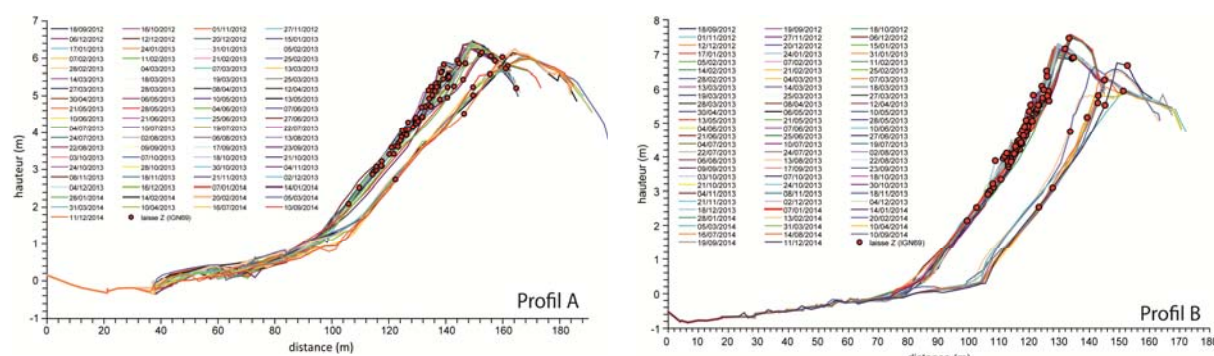


Figure C - Enveloppe de profils topo-morphologiques et positionnement de la laisse de mer au niveau des profils A et B entre les mois de septembre 2012 et décembre 2014 (Fichaut et al., 2015).

L'apport des mesures à haute fréquence avait de plus permis de voir que ce recul s'était en 3 temps correspondant à l'impact de 3 tempêtes combinées à une marée de vive-eau (figure D).

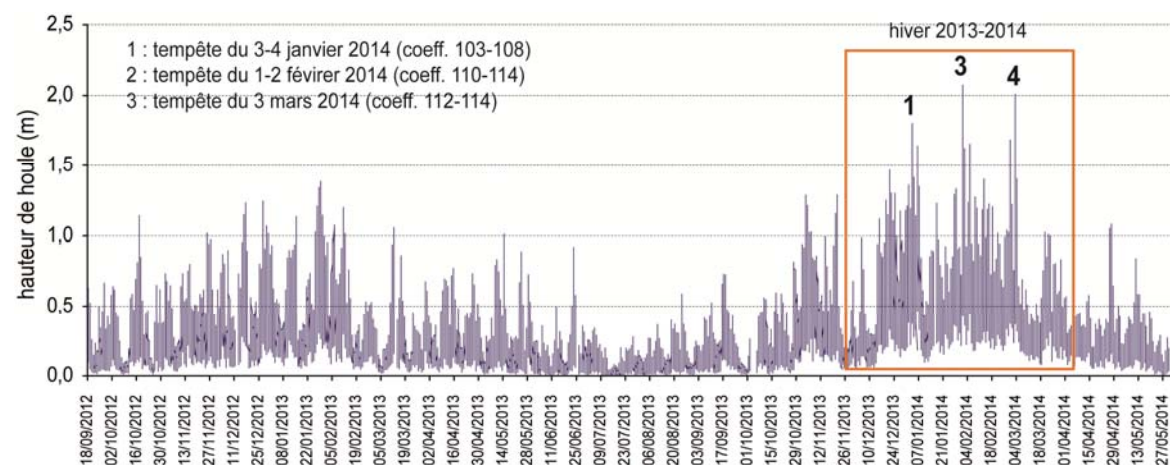


Figure D – Enregistrement de hauteur de houle à partir du capteur de pression installé dans la zone intertidale au droit du profil B, montrant les 3 épisodes tempétueux majeurs de l'hiver 2013-2014 (Fichaut et al., 2015).

Le premier épisode morphogène du début du mois de janvier (3-4 janvier), combiné à une marée de 103-108, a généré un recul peu important : entre  $-4$  et  $-5$  m. Le second du début du mois de février (1-2 février), combiné à une marée de 110-114, s'est soldé par un recul plus important atteignant  $-10$  à  $-14$  m. Le troisième épisode correspondant à la tempête Christine du 3 mars, associée à une marée de 112-114, a généré un recul d'environ  $-5$  m (figure E).

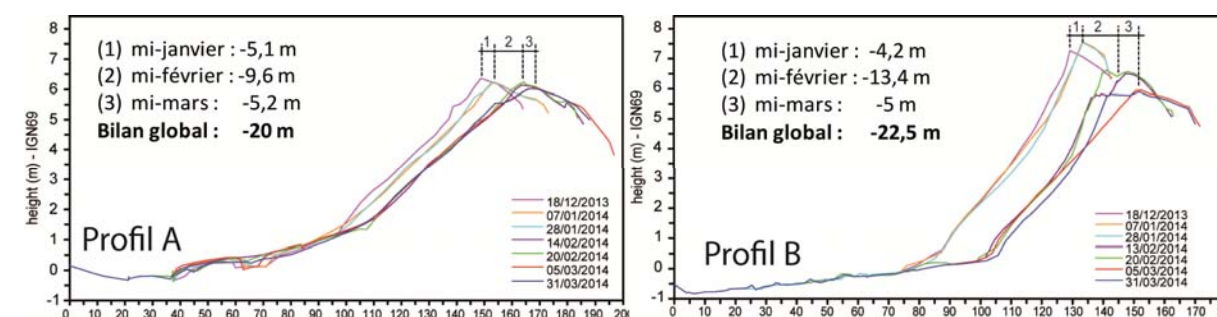


Figure E : Recul du sillon de Talbert entre les mois de décembre 2013 et mars 2014 restituée à partir des levés topo-morphologiques à haute fréquence le long des profils A et B (Fichaut et al., 2015).

#### 4.2- Bilan depuis l'hiver 2013-2014 (mars 2014 - janvier 2018)

Les levés effectués depuis le mois de décembre 2014 ont permis d'analyser le comportement morphologique du Sillon de Talbert après cet hiver particulièrement morphogène. Ainsi, entre les mois de janvier 2015 et 2018, 17 levés topo-morphologiques ont été réalisés le long des deux profils A et B (figure F et G).

L'évolution morphologique globale montre plusieurs phases que l'on peut décrire comme suit. Au niveau du profil A, entre le mois de mars 2014 (date de la dernière tempête de l'hiver 2013-2014) et le mois de décembre 2017, le cordon n'a fait que s'exhausser (figure Gb). Cet exhaussement de la crête d'environ  $+40$  cm s'est fait au détriment de la face avant du cordon qui a perdu du sédiment, notamment en bas de profil. Cela s'explique par l'action des petites houles de temps plutôt calme qui ont remonté le matériel du bas du profil vers la crête afin de lui redonner sa pente d'équilibre post-tempête. Entre le mois de décembre 2017 et le 5 janvier 2018 (date du dernier levé), le profil externe du cordon a reculé dans son ensemble, et la crête s'est de nouveau abaissée d'environ  $-40$  cm ; une partie du matériel perdue par la crête est passée sur la face arrière qui montre une nette accrétion (figure Fc). Ces changements morphologiques sont liés à l'impact de la tempête Eleanor du 3 janvier 2018 (vitesses de vents de plus de  $125$  km/h ont été enregistrées à la station météo-France de Brignogan), combinée à une marée de vive-eau de 106-107.

Au niveau du profil B, l'évolution est un peu plus complexe ; elle s'articule autour de 4 phases. Entre les mois de mars 2014 et de d'octobre 2015, le profil s'est exhaussé d'environ  $1,25$  m (figure Gb). Là encore, l'exhaussement de la crête s'est fait à partir du matériel érodé sur la face externe du cordon, notamment en bas de profil. Le levé du 16 février 2016 réalisé après la tempête Imogen-Ruzica du 8 février 2016 montre un net recul du cordon associé à un écrêtement de ce dernier ( $-0,80$  m), et d'une accrétion sur le revers (figure Gb). La troisième phase (entre les mois de février 2016 et décembre 2017) est marquée par un nouvel exhaussement du cordon ( $+0,65$  m) au détriment de la face externe qui s'érode en bas de profil (figure Gc). La quatrième et dernière phase est liée à l'impact érosif de la tempête Eleanor du 3 janvier 2017. Comme pour le profil A, cet épisode a entraîné un nouvel abaissement de la crête ( $-1,30$  m), associé à un recul complet du cordon et une accrétion importante du revers



(figure Gd). Cette évolution morphosédimentaire illustre là encore le phénomène de roulement transversal (*rollover*) du cordon sur lui-même sous l'effet de la submersion lors des tempêtes.

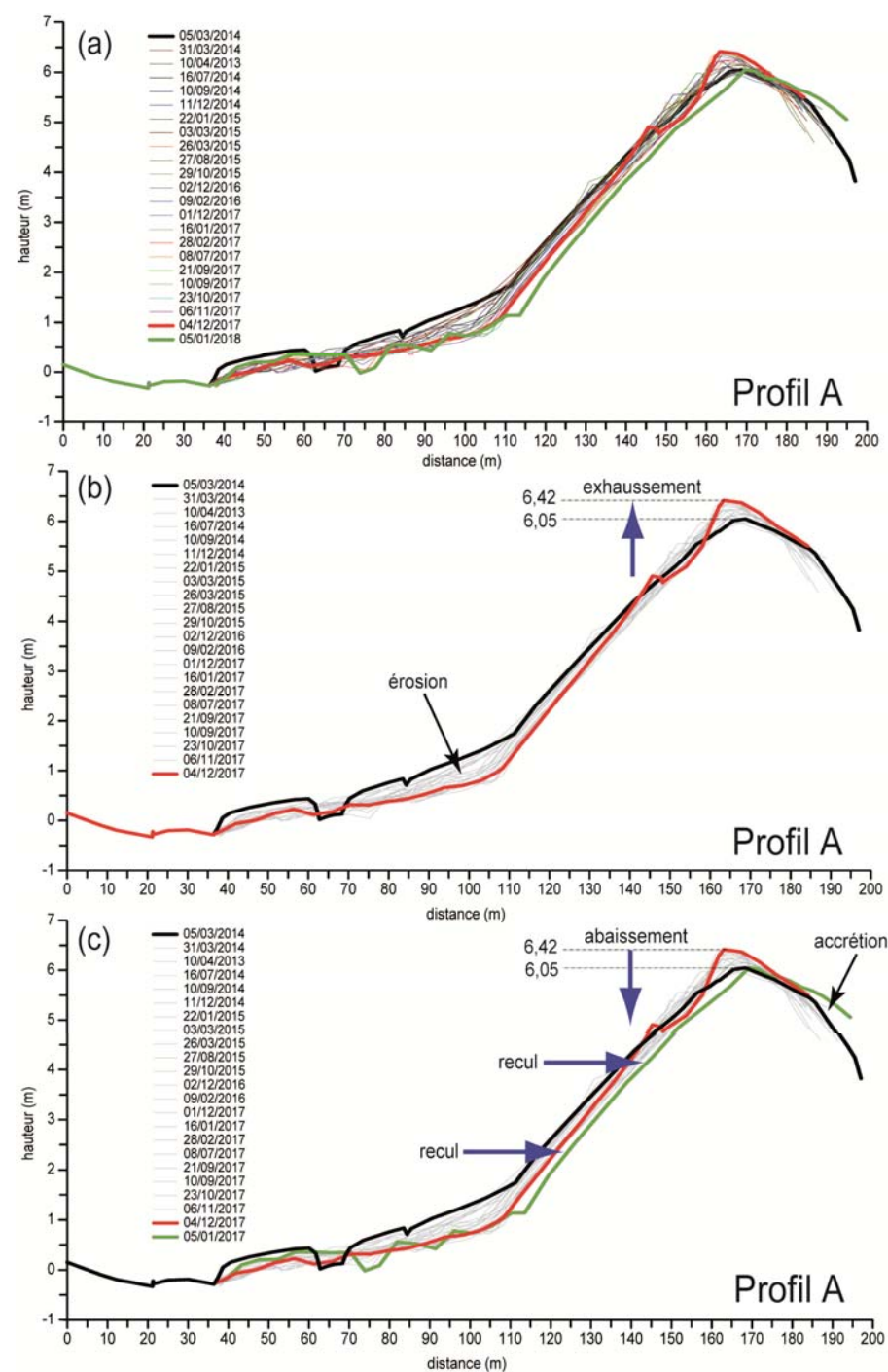


Figure F – Evolution morphologique du sillon le long du profil A entre les mois de mars 2014 et janvier 2018

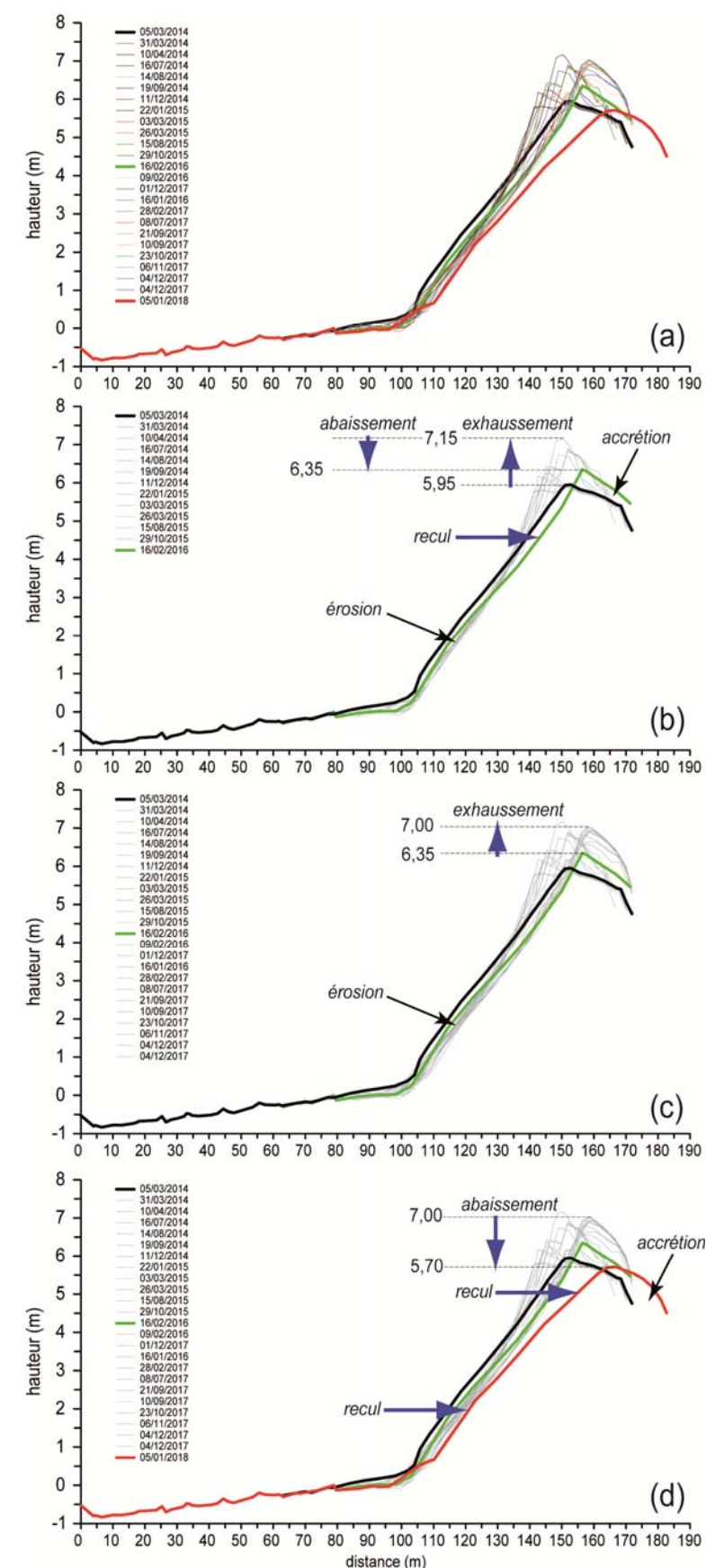


Figure G – Evolution morphologique du sillon le long du profil B entre les mois de mars 2014 et janvier 2018

#### 4.3- Conclusion sur le suivi à haute fréquence

Le suivi à haute fréquence réalisé depuis 2012 montre une tendance au recul le long des deux profils A et B : -20 m et -40 m respectivement (figure H). L'hiver 2013-2014 constitue toutefois l'évènement majeur dans cette évolution. Dans le détail, les processus morphosédimentaires mesurés illustrent le fonctionnement classique de roulement des cordons (*rollover process*) sous l'effet des submersions de tempête. Ces dernières génèrent une érosion du haut du profil associée à un écrêtement ; le matériel érodé vient s'accumuler sur le revers entraînant une diminution de la pente externe du cordon. Les processus post-tempêtes (associés aux houles peu énergétiques de beau temps) interviennent dans le redressement du cordon. Ce mécanisme se traduit par une érosion du bas du profil externe dont le matériel remonté par les petites houles participe à l'accrétion du haut du profil et de la crête sommitale qui s'exhausse. Le bilan de ce fonctionnement se solde par un déplacement complet du cordon vers la terre sans que son volume sédimentaire global n'en soit affecté.

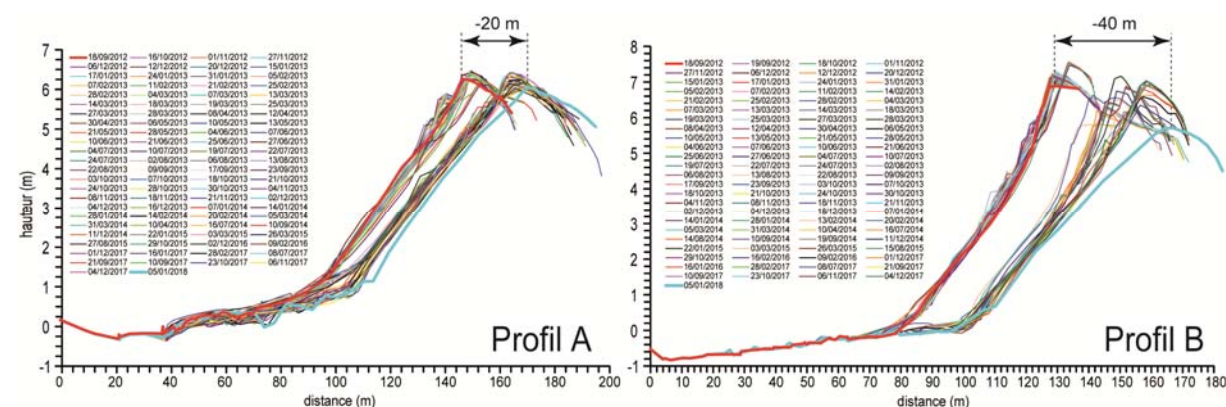


Figure H – Bilan du recul du sillon de Talbert le long des profils A et B entre le 18 septembre 2012 et le 5 janvier 2018.

## 5- Références bibliographiques

Blaise E., Suanez S., Stéphan P., Fichaut B., David L., Cuq V., Autret R., Houron J., Rouan M., Floc'h F., Arduind F., Cancouët R., Davidson R., Costa S., Delacourt C. - Bilan des tempêtes de l'hiver 2013-2014 sur la dynamique de recul du trait de côte en Bretagne. *Géomorphologie : relief, processus, environnement*. 21 (3), pp. 267-292.

Fichaut B., Suanez S., Stéphan P., (2010) – Rapport sur le suivi morphosédimentaire du Sillon de Talbert pour l'année 2010, décembre 2010, 16 p.

Fichaut, B., Stéphan P., Suanez, S., Blaise E. (2013) – Suivi topo-morphologique du Sillon de Talbert (Commune de Pleubian - Période 2012-2013), 27 p.

Stephan P., Fichaut, B., Suanez, S. (2007) – Rapport d'activité sur le suivi topo-morphologique du Sillon de Talbert (Commune de Pleubian), 19 p.

Stephan P., Fichaut, B., Suanez, S. (2008) – Deuxième rapport d'activité sur le suivi topo-morphologique du Sillon de Talbert (Commune de Pleubian - Période 2007-2008), 12 p.

Stephan P., Fichaut, B., Suanez, S. (2009) – Suivi topo-morphologique du Sillon de Talbert (Commune de Pleubian - Période 2008-2009), 10 p.

Stephan P., Fichaut, B., Suanez, S., Blaise E. (2011) – Suivi topo-morphologique du Sillon de Talbert (Commune de Pleubian - Période 2010-2011), 10 p.

Stephan P., Fichaut, B., Suanez, S., Blaise E. (2012a) – Suivi topo-morphologique du Sillon de Talbert (Commune de Pleubian - Période 2011-2012), 14 p.

Stéphan P., Suanez S., Fichaut B. (2012b) – Long-term morphodynamic evolution of the Sillon de Talbert gravel barrier spit, Brittany, France, *Shore & Beach*, 80, 1, pp. 19-36.

Stéphan P., Fichaut B., Suanez S., Blaise E., Autret R. (2015) – Rapport sur le suivi topo-morphologique du Sillon de Talbert pour l'année 2014, mars 2015, 32 p.

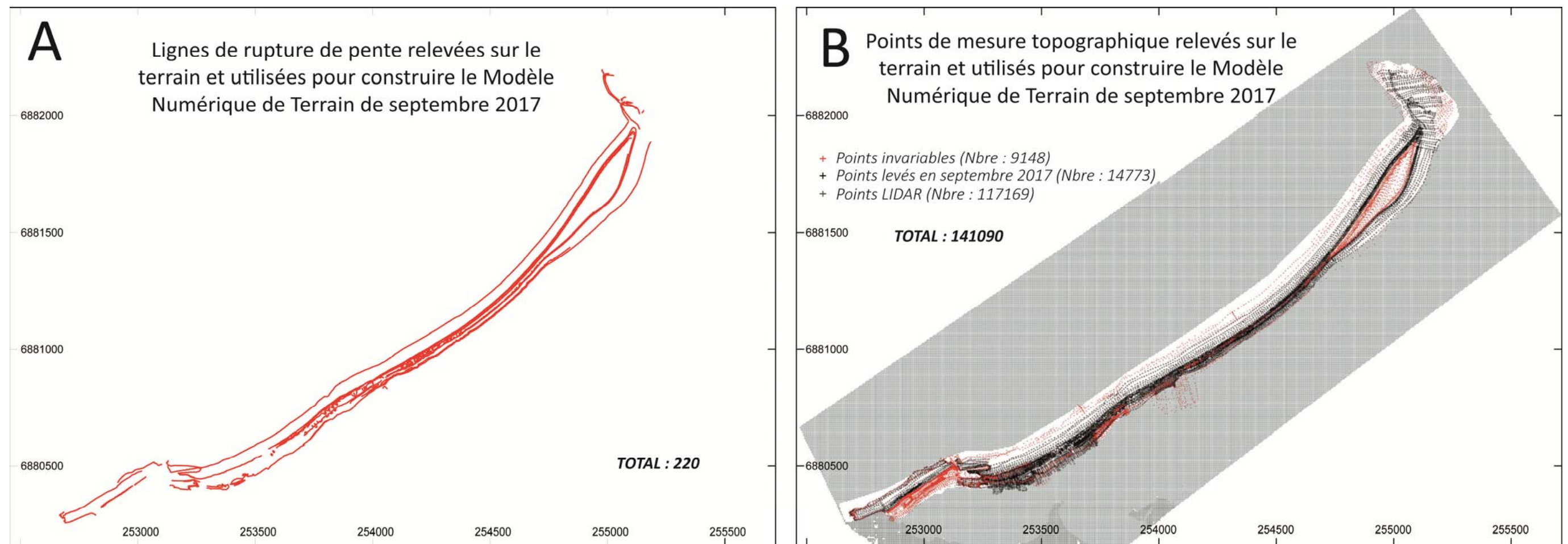


Figure 1 : Données topographiques utilisées pour construire les modèles de terrain de septembre 2017 sur le Sillon de Talbert.

A. Localisation des lignes de rupture de pente relevées. B. Localisation des points topographiques utilisés.

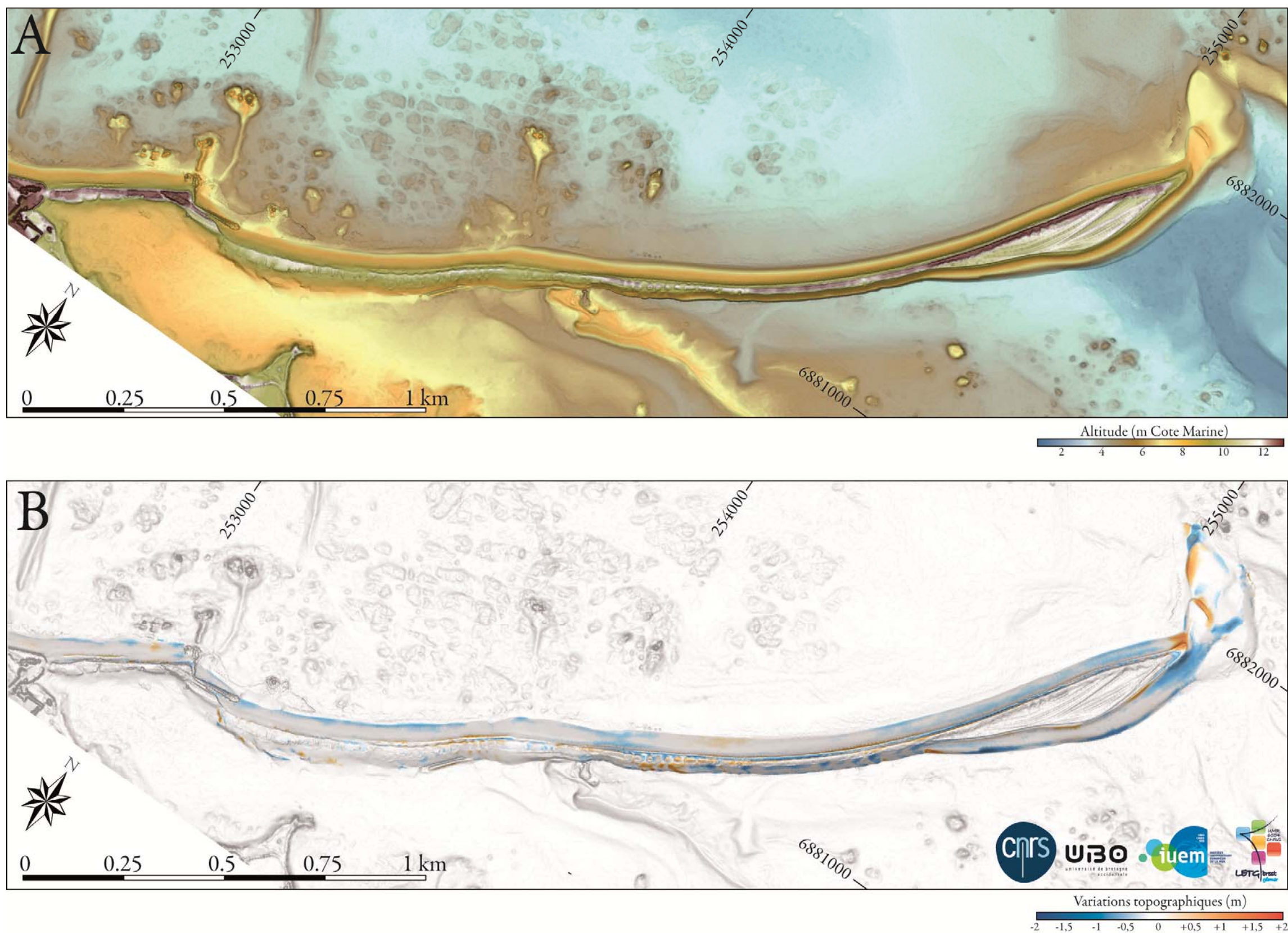


Figure 2 : Modèle Numérique de Terrain du Sillon de Talbert en septembre 2017 (A). Evolution topo-morphologique du Sillon de Talbert entre octobre 2016 et septembre 2017.

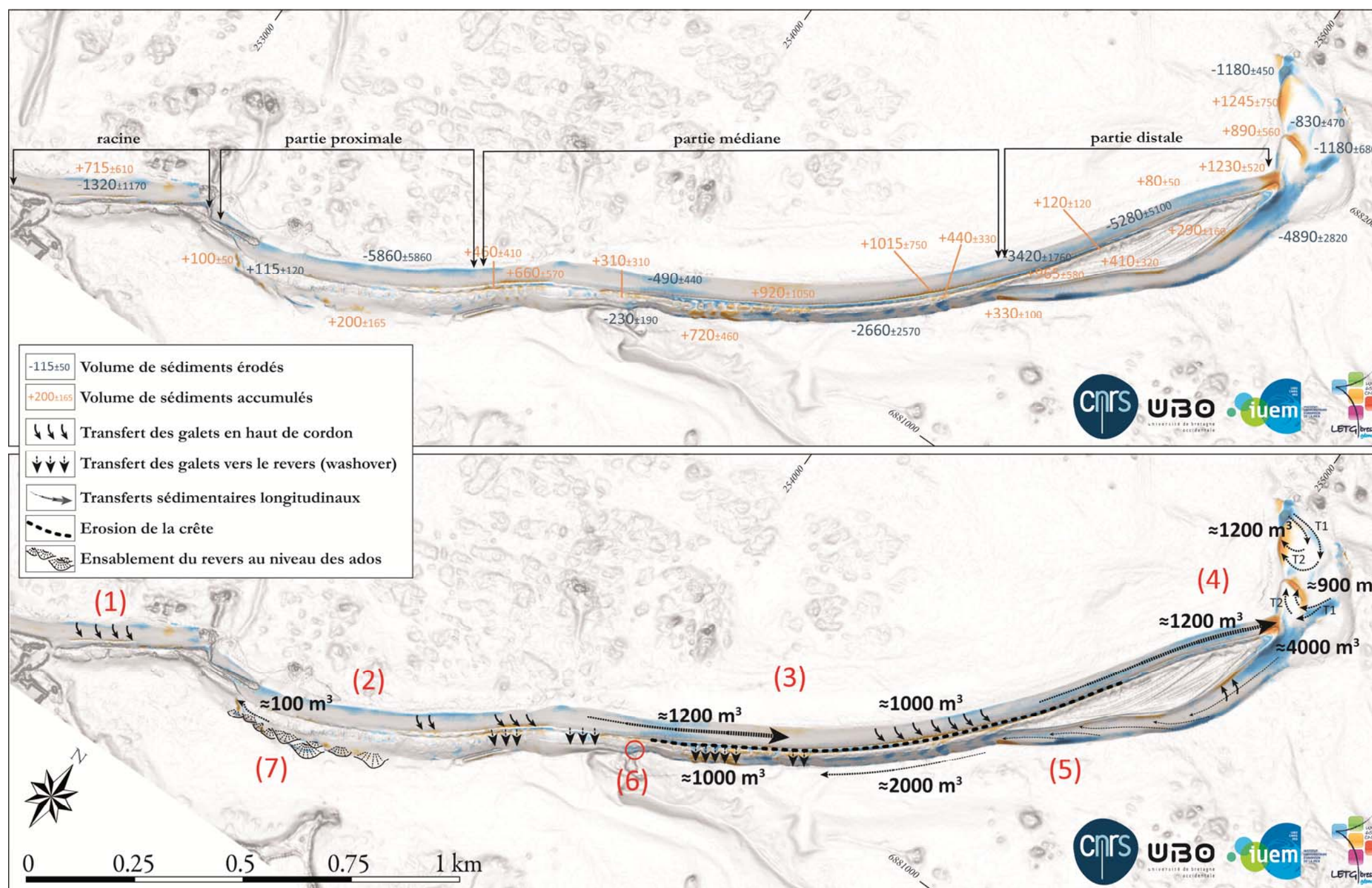


Figure 3 : Dynamiques morphosédimentaires sur le Sillon de Talbert entre octobre 2016 et septembre 2017.

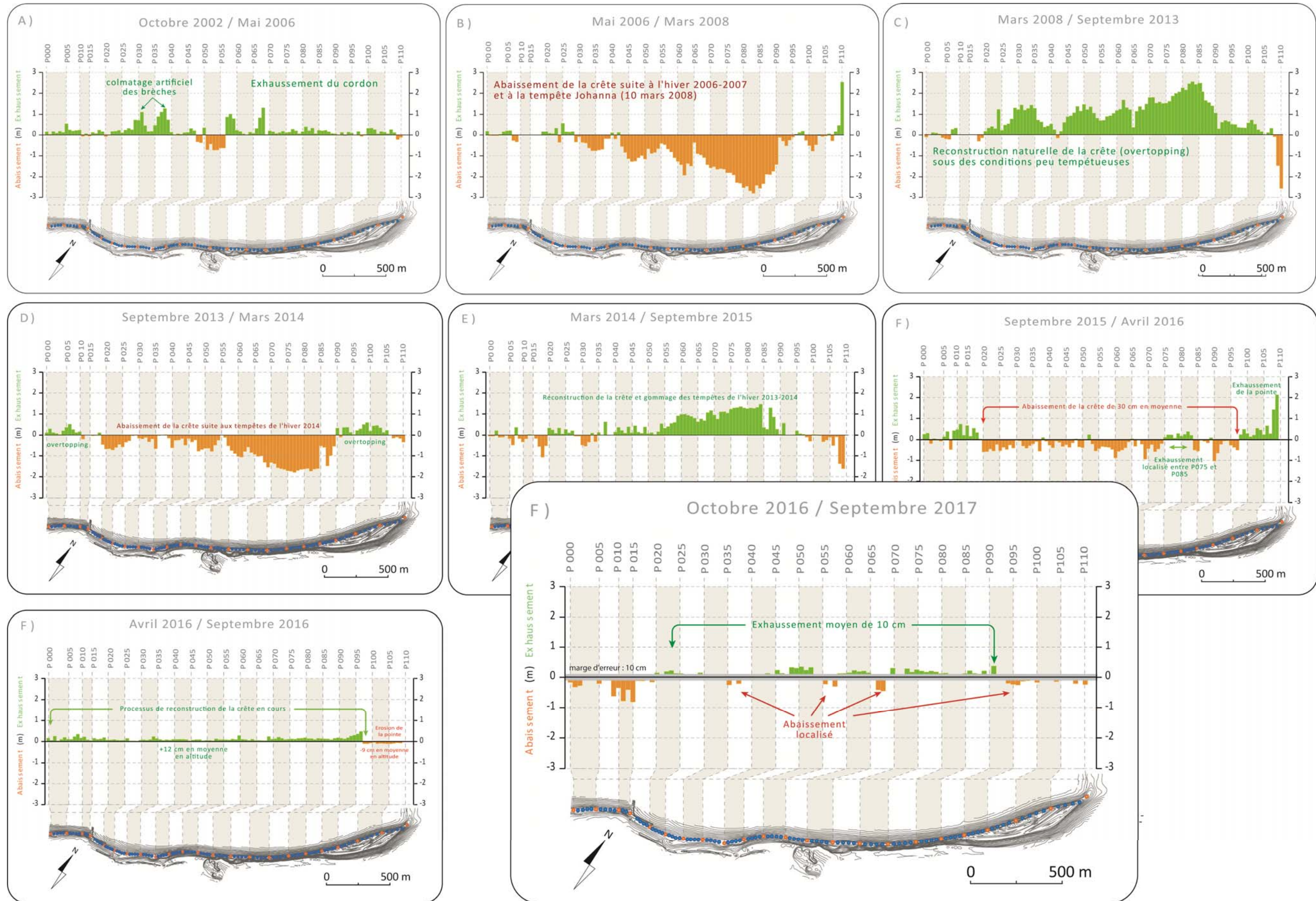


Figure 4 : Variations de l'altitude de la crête du Sillon de Talbert.

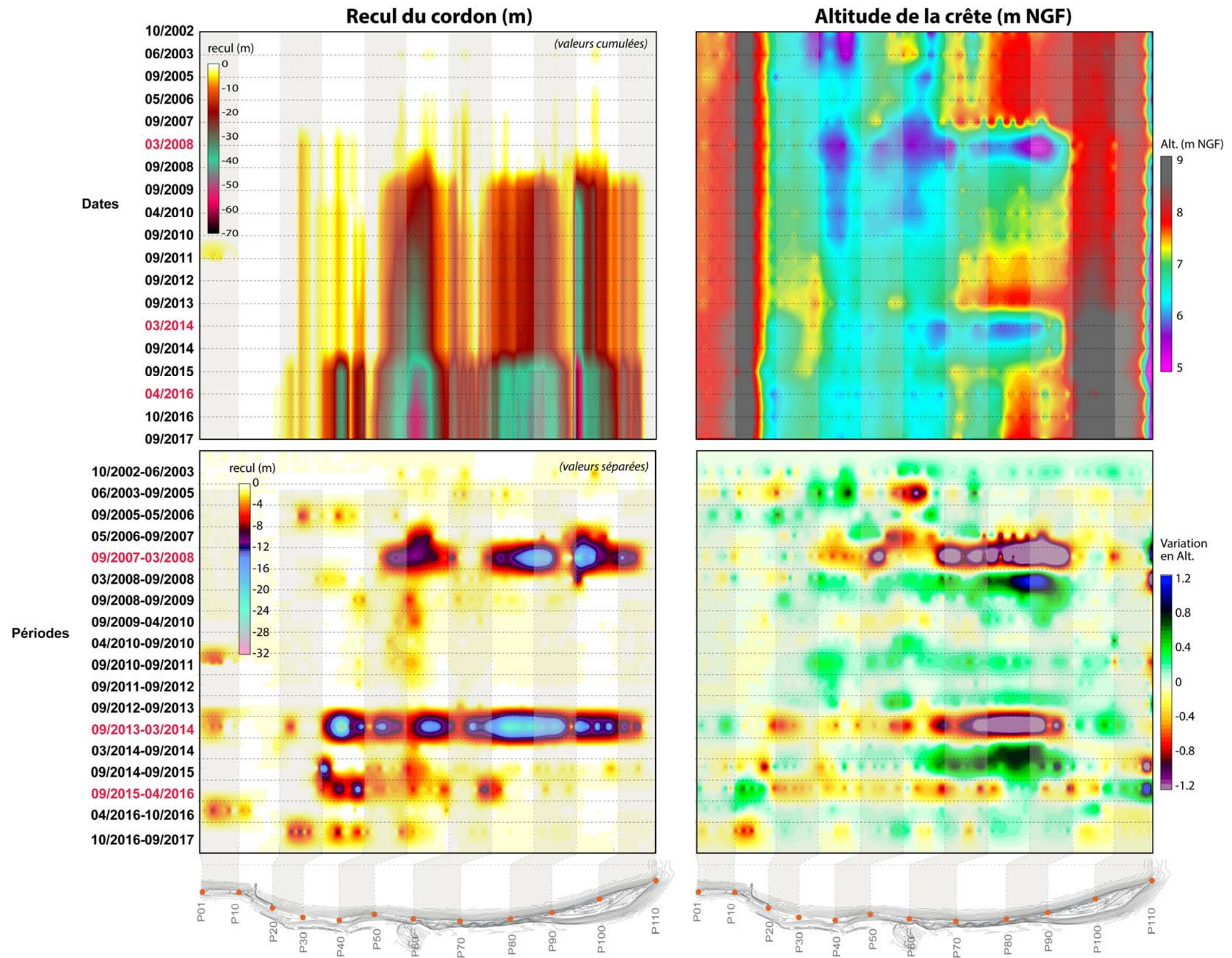


Figure 5 : valeurs du recul et de la hauteur du sillon de Talbert depuis le début des suivis en 2002.

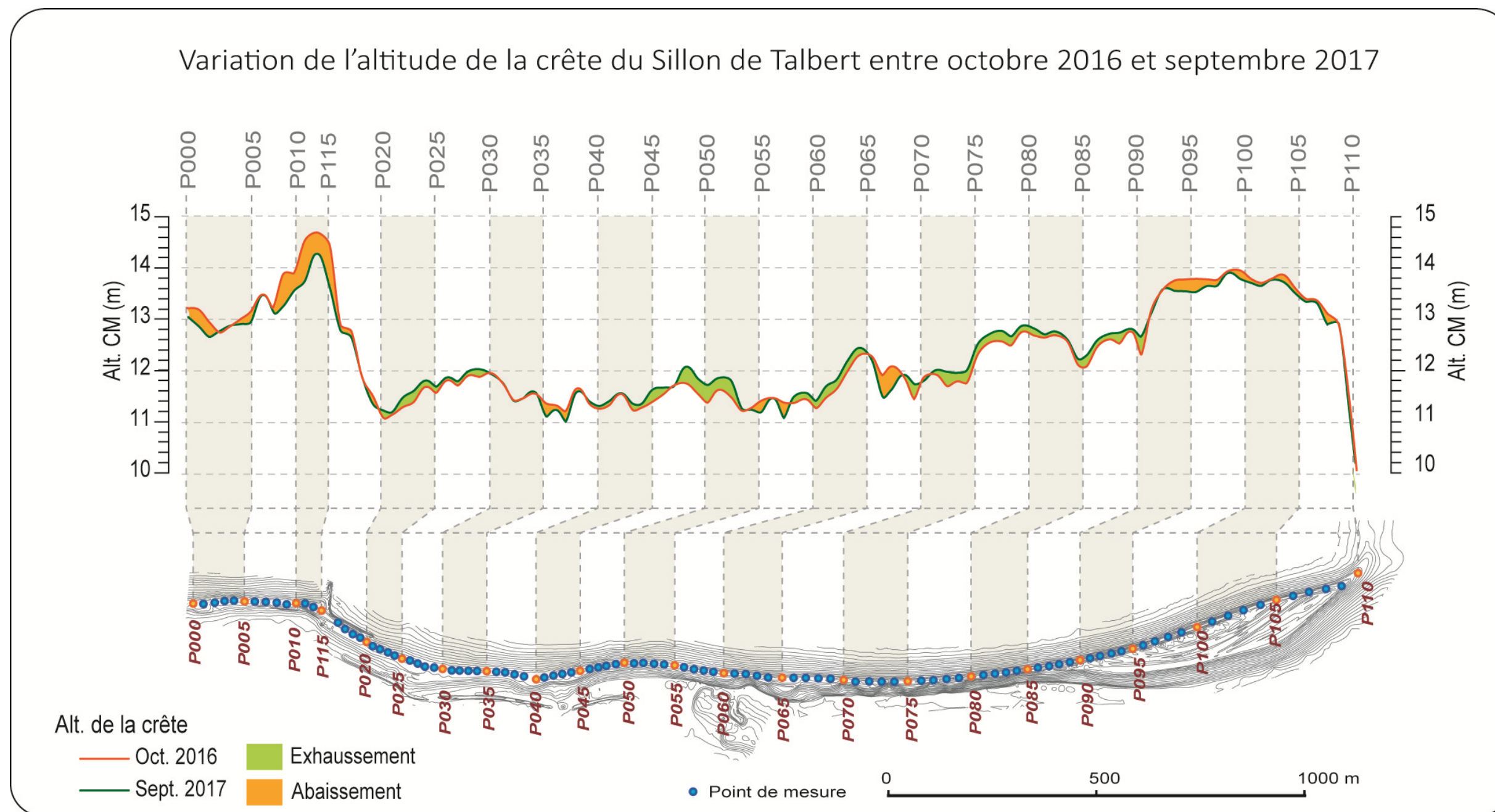


Figure 6 : Variations de l'altitude de la crête du Sillon de Talbert d'octobre 2016 à septembre 2017.



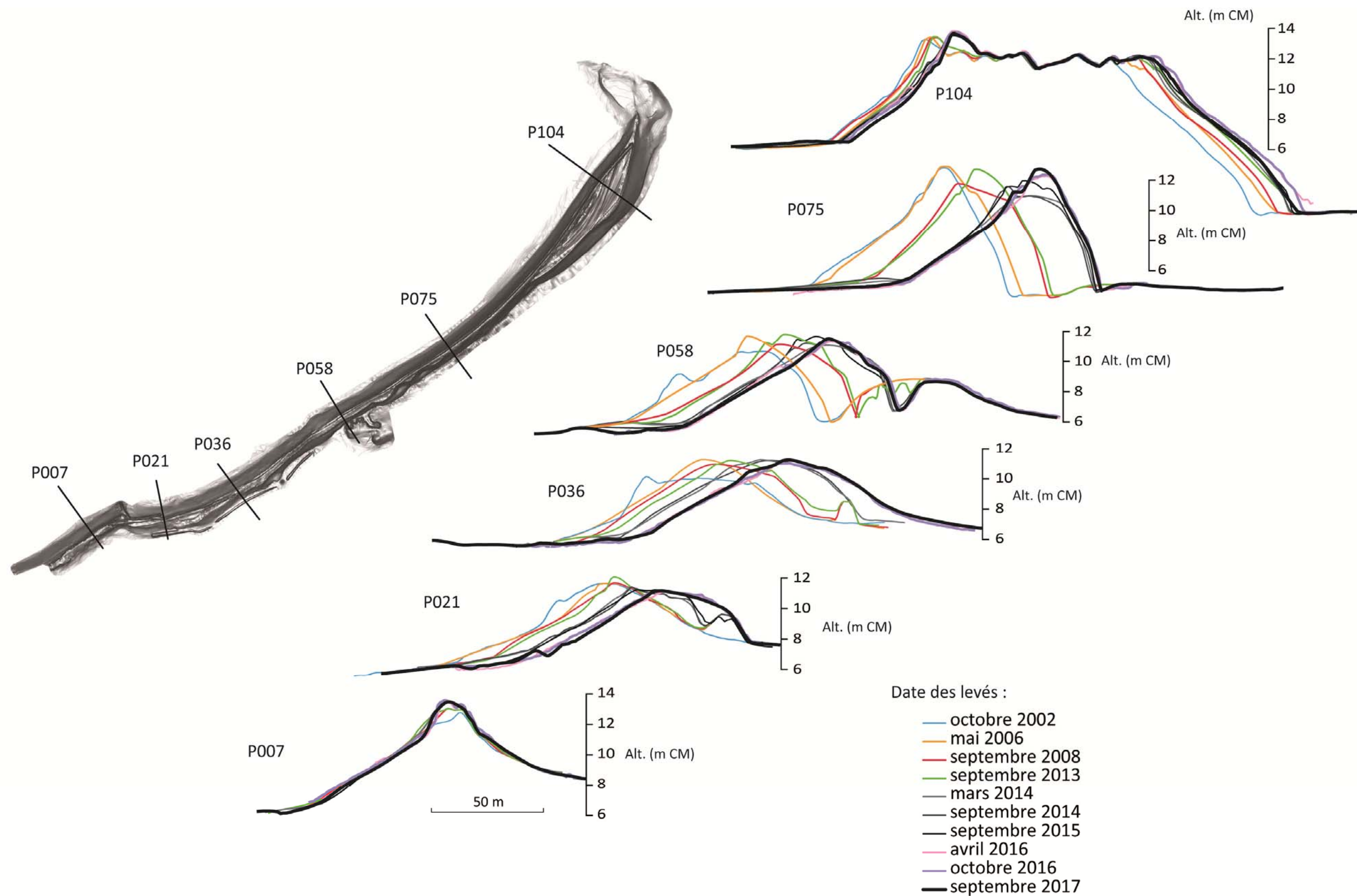


Figure 7 : Evolution des profils transversaux du sillon de Talbert.

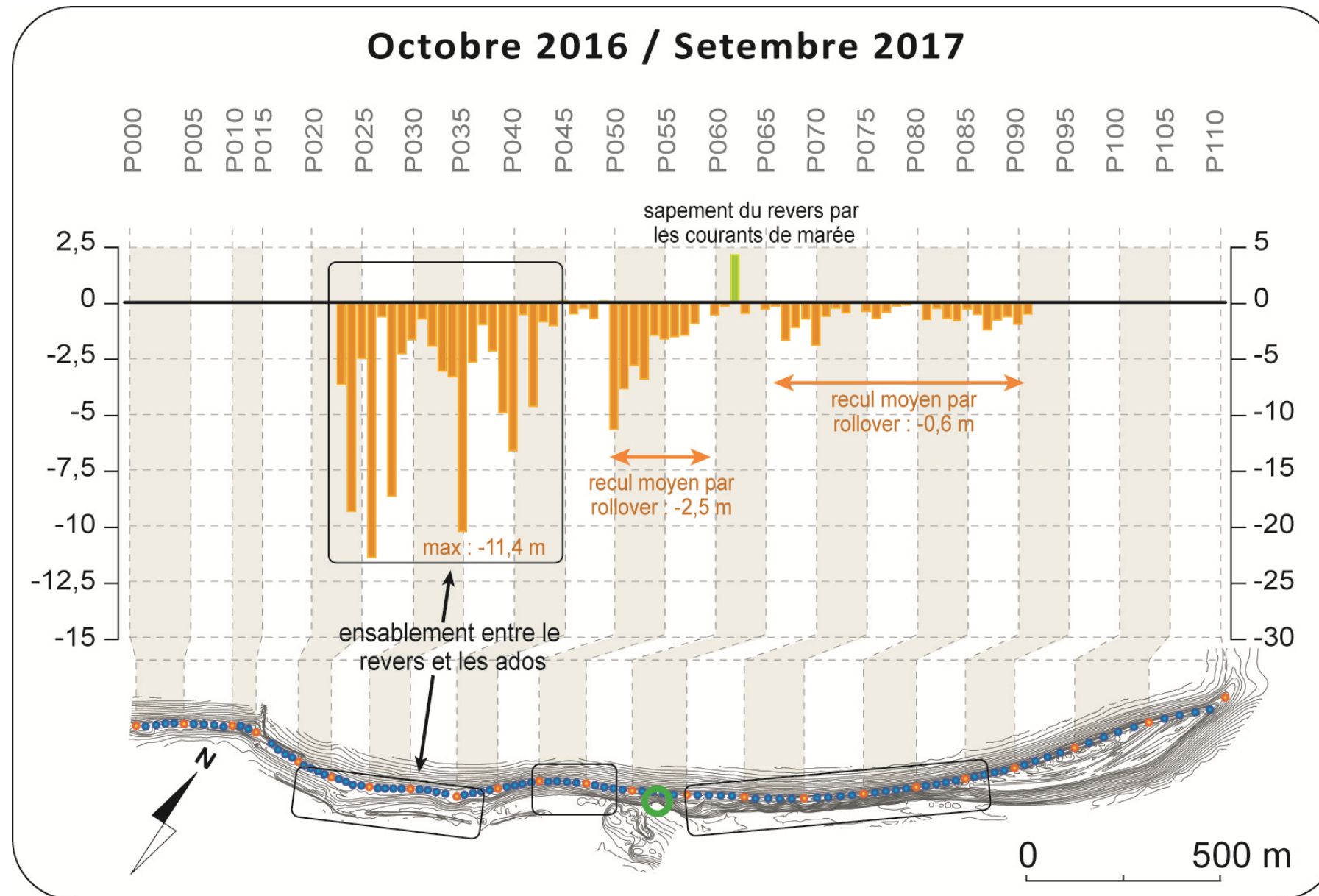


Figure 8 : Recul de la base du revers du Sillon de Talbert entre octobre 2016 et septembre 2017.

# Monitoring the medium-term retreat of a gravel spit barrier and management strategies, Sillon de Talbert (North Brittany, France)

Pierre Stéphan<sup>1,2</sup>, Serge Suanez<sup>2</sup>, Bernard Fichaut<sup>2</sup>, Ronan Autret<sup>2</sup>, Emmanuel Blaise<sup>2</sup>, Julien Houron<sup>3</sup>, Jérôme Ammann<sup>4</sup>, Philippe Granjean<sup>5</sup>

<sup>1</sup>CNRS, Université de Bretagne Occidentale, UMR LETG 6554, Institut Universitaire Européen de la Mer, Plouzané, France

<sup>2</sup>Université de Bretagne Occidentale, CNRS, UMR LETG 6554, Institut Universitaire Européen de la Mer, Plouzané, France

<sup>3</sup>Réserve naturelle régionale du Sillon de Talbert, 22610 Pleubian, France

<sup>4</sup>CNRS, Université de Bretagne Occidentale, UMR LGO 6538, Institut Universitaire Européen de la Mer, Plouzané, France

<sup>5</sup>Université de Lyon 1 et ENS-Lyon, CNRS, UMR 5570, 69662 Villeurbanne, France

<sup>6</sup>Université de Bretagne Occidentale, CNRS, UMR LGO 6538, Institut Universitaire Européen de la Mer, Plouzané, France

Email: pierre.stephan@univ-brest.fr, serge.suanez@univ-brest.fr, bernard.fichaut@univ-brest.fr, \*maison-littoral-pleubian@orange.fr, jerome.ammann@univ-brest.fr, Philippe.Granjean@univ-lyon1.fr

## Highlights

- 1-Topo-morphological monitoring and management strategies
- 2-Increase of spit landward retreat over the last fifteen years
- 3-Dominant cross-shore dynamic due to storm event washover
- 4-Longshore transfers through cannibalization process
- 5-Beach replenishment as coastal management option

**Keywords:** Gravel spit barrier; topo-morphological monitoring; landward retreat; storm; management strategies; replenishment

## Abstract

The Sillon de Talbert is a large swash-aligned gravel barrier spit of 3.5 km length, situated on the Northern coast of Brittany. Over the last decades, the spit experienced landward migration by rollover reaching 1.1 m.yr<sup>-1</sup> at least since 1930, with maximum retreat rates of 1.35 m.yr<sup>-1</sup> affecting the proximal section. This evolution has led to the construction of coastal defense structures (rip-rap and groin) during the 70's and 80's to stabilize the spit. In 2001, when the Sillon de Talbert became the property of the French public office called "*Conservatoire du Littoral*", a different management strategy led to the removal of these hard coastal defence structures. At the same time, a topo-morphological survey was undertaken to analyze and quantify both cross-shore and longshore morphosedimentary processes of the spit. This monitoring began in 2002 and is still ongoing. The results show that the spit landward displacement has increased during the last fifteen years with rates of retreat almost twice as great as prior to 2002 when the monitoring began (2 m.yr<sup>-1</sup> vs 1.2 m.yr<sup>-1</sup>). The most efficient migration process occurs when a high tide level coincides with storm waves inducing sluicing overwash and/or inundation regime. In that context, the spit barrier retreat reaches several tens of meters through rollover processes. However, following such episodes of

overwashing the crest of the spit may rise rapidly during fair meteorological periods. Longshore sediment transfer through cannibalization processes is also driving the evolution of the Sillon de Talbert. Due to both of these dynamics, the spit is actually threatening to break in its proximal section in a zone called “wasp waist” where the landward retreat has been the most important since the survey began in 2002. Two strategies in terms of coastal erosion management are drawn according to the policy of the “*Conservatoire du Littoral*”, as owner of the Sillon de Talbert area, and the duty of the municipality of Pleubian to manage the coastal risks on its communal land. The first option is to remove the existing hard coastal defence structures in order to allow the spit to recover its natural morphodynamic. This option would imply the relocation of several buildings to prevent coastal erosion/flooding risk due to the withdrawal of coastal defence structures. The second option consists of sediment replenishment in the threatened zone with pebbles extracted from available sediment sources. The topo-morphological survey provided relevant scientific expertise in terms of volumetric requirements and existing sources to support this option.

## **1. Introduction**

Gravel spit barriers are depositional bar or beach landforms off coasts. Therefore, they are widely regarded as effective and sustainable forms of coastal defense. Therefore, an understanding of their morphosedimentary functioning and evolution is essential in terms of coastal management (Hudson and Baily, 2018). The profile of gravel barriers generally exhibits a gentle seaward beach-face suitable to dissipate large amounts of wave energy (McCall et al., 2015), while the landward beach slope is steep and dips to the rear of the spit form. According to the classifications of Zenkovich (1967) and Davies (1972), the geometric plan-view morphologies show both situations of drift-aligned and swash-aligned barriers. Orford et al. (1996) showed that the swash-aligned barriers often represent the final stage of the morphological development of the gravel barriers associated with a scarcity of longshore sediment supply. Therefore, the morphology, sediments, and dynamic processes of gravel barriers are controlled by both cross-shore and longshore dynamics (Orford et al., 2002; Orford and Anthony, 2011).

Gravel spit barriers –notably swash-aligned barriers– most often present a single crest and are highly sensitive to landward migration due to rollover processes operating over short term (daily-to-monthly time scale related to storm conditions), and decades-to-century-to-millennium-scale time scales driven by relative sea-level change (Carter and Orford, 1984 ; Orford et al. 1991, 1995 ; Orford and Carter, 1995). However, significant rollover processes occur during extreme events when wave runup overwashes, or strongly inundates the crest of the barrier (Donnelly et al., 2006). Several authors have proposed storm-impact scaling models to characterize the response of the barriers to the storms or hurricanes. On gravel-dominated deposits, four types of impact level to overwash process have been recognised by Orford and Carter (1982). First, an “*overtopping*” process is observed when runup reaches the barrier crest. The infiltration of the uprush in the sediment diminishes the intensity of the backwash generating an accretion phenomenon of the crest (Holman et Sallenger, 1985 ; Butt et Russel, 2000 ; Masselink et Li, 2001 ; Buscombe et Masselink, 2006). The second type occurs

when the extreme water level passes over the crest inducing a “*discrete overwash*” process that slightly erodes the top of the crest. The third type is described as a complete removal of the crest caused by a “*sluicing overwash*” process involving high extreme water level that generates a competent and unidirectional flow largely unaffected by percolation. In that case, the crest is lowered due to erosion and small-scale back-barrier washover fan deposition is observed. Finally, during an intense storm event, as the swash limit rises during the storm, the sluicing overwash evolves into “*overwashing*” processes. In that case, depositional washover activity is observed on the beach crest in the form of breach or throat plug sedimentation, as well as on the back-barrier in the form of washover fans and splays. Following the same approach, Sallenger (2000) and Stockdon et al. (2007) identified four impact levels that included a “*swash*” regime (impact level 1), a “*collision*” regime (impact level 2), an “*overwash*” regime (impact level 3), and culminates in an “*inundation*” regime (impact level 4) when the storm surge is sufficient to completely and continuously submerge the barrier. Therefore, overwash is the fundamental mechanism forcing barrier retreat through rollover processes under long-term sea-level rise or repeated yearly storm events (Orford et al., 1995; Jiménez and Sánchez-Arcilla, 2004; Stéphan et al. 2010; Benavente et al., 2013; Tillmann and Wunderlich, 2013)

The longshore dynamic is also one of the main factors controlling the functioning and the evolution of the gravel spit barriers. It depends on the balance between the potential longshore transport ( $Q_y$ ) rate as an energy term, dependent on the angle of breaker approach ( $\alpha$ ), and the availability of sediment to be transported along the shore by this energy (Orford et al., 2002). Therefore, a drift-aligned barrier is associated with sediment transport rate  $Q_y > 0$ , while a barrier in swash-aligned status is associated with  $Q_y \approx 0$ . The shift from drift-aligned to swash-aligned status is ultimately dependent on sediment supply, though wave climate variations may also be influential. When the sediment supply is depleted the wave energy reworks existing beach deposits through cannibalization (Carter and Orford, 1993); at the same time, the incident breaker is refracted so that it breaks along the entire beach at the same time, inducing a perfect swash alignment ( $\alpha = 0$ ) and a potential longshore transport  $Q_y = 0$  (Orford et al., 2002).

The Sillon de Talbert is governed by these both dynamics. The landward migration of the spit due to rollover processes have been observed since the 18th century (Pinot 1994). However, it was after the large landward displacement (associated to large breaches) of the proximal section by the major storm of 5 April 1962 that stabilization operations of the spit were undertaken. A 400 m long rip-rap and a groin called “*Chouck groin*” were built in 1974 in order to protect/stabilize the proximal section. By the end of 1970’s, a second 1100 m long rip-rap defense structure was also built on the top of the barrier of the medium section to prevent storm overwash and stop the rollover processes. In 1982, this frontal armor was extended toward the distal section over 300 m long (Pinot, 1994; Stéphan et al., 2012). However, these coastal defense structures quickly appeared ineffective; in addition, they have hindered the natural self-organization processes of the spit such as the impediment of the rise of the crest by overtopping, or the increase of wave reflection leading the erosion of the lower beach face. At the beginning of 1990’s, the frontal dyke was completely disconnected seaward from the spit due to landward migration and the longshore sediment transport through cannibalization generated significant erosion on the proximal/medium zone while the distal

section gained in sediment (Pinot 1994; Stéphan et al. 2012). In 2001, the management of the Sillon de Talbert was transferred to the public trust “*Conservatoire du Littoral*”, which adopted a different coastal erosion management strategy. The rip-rap was removed in order to allow the gravel spit barrier to recover its natural morphodynamic. At the same time, a topo-morphological survey was undertaken to analyze and quantify both cross-shore and longshore morphosedimentary processes of the spit. This paper presents the results obtained from this topo-morphological survey. According to these results, some recommendations in terms of soft managing solution are proposed.

## 2. Study site

The Sillon de Talbert is a gravel spit barrier located on the south-west coast of the English Channel, in Northern Brittany (France) (Fig. 1). It is part of the “*Réserve Naturelle Régionale du Sillon de Talbert*” created in 2006 by the Brittany Region and the French State. It extends over 250 hectares including the spit and the surrounding intertidal area (Fig. 1c). In addition the “*Conservatoire du littoral*” has established a preemption area on the privately owned lands bordering the southern limit of the reserve. Three stakeholders establish the management plan for a period of five years: Brittany region, Conservatoire du littoral, municipality of Pleubian. The latter is in charge of the implementation of the management actions.

The Sillon de Talbert forms a 3.5 km long, single-ridge gravel spit barrier. The sediment volume is estimated at  $1.23 \cdot 10^6 \text{ m}^3$  (Stephan, 2011). The barrier can be classified in the type of “composite gravel beaches” (Orford and Carter, 1982; Jennings and Shulmeister, 2002). The beach face is characterised by a break slope point at the mean water level. The lower part of the beach face has a low slope gradient (0.01%), and corresponds to a large rocky platform partially covered by periglacial deposits and/or scattered recent sandy sheets. The upper part of the beach face shows steeper slopes, ranging between 5% and 15%. The gravel barrier can be subdivided into four distinct morphosedimentary units (Fig. 2). Unit 1 corresponds to the proximal sandy section mainly composed of fine to medium sand material (pebbles fraction < 30%). The slope gradient is between 5% and 8%. The crest height exceeds 8.5 m above mean tide level (a.s.l) in places due to the formation of dunes on the top of the barrier (Fig. 2b). This section is sheltered by many rocky outcrops located in front on the rocky platform. The upper-beach/dune zone is artificially protected by a rip-rap over a distance of 120 m, and a groin called “*Chouck groin*” has been installed at the end of the cell to prevent loss of sediments due to longshore drift oriented to the NE (Fig. 3a). Because of the difference of sediment size and morphology (e.g. mainly sandy and existence of the dunes) and the presence of the coastal defense structures, this section will not be studied in this paper. Unit 2 is the proximal gravel section composed by a mixed sand and pebbles (pebbles fraction <40%). The barrier presents a low slope gradient (between 5% and 7%). The crest shows small-size embryonic sand dunes and the elevation is around 6 m a.s.l. (Fig. 2b). Unit 3 correspond to the median section. The sediment material is mainly composed of pebbles

(pebbles fraction >70%). The beach slopes are steeper and the crest is about 7 m a.s.l. (Fig. 2b). Unit 4 forms the distal section of the Sillon de Talbert. It corresponds to the accretion zone of the spit downdrift of the longshore sediment transport. Here, the net positive sediment supply explains the enlargement of the tip back-barrier which is characterized by accreted ridges due to wave diffraction (Fig. 3b). The pebble fraction exceeds 80%. The beach-face slope increases to 15% while the elevation of the crest reaches 7.5 m a.s.l. Due to this slope, this section is the most reflective part of the spit characterized by the formation of beach cups. Finally, a fifth unit may be identified at the end of the tip of the spit; it concerns the large ebb tide delta that stretches to the North-West (Fig. 3b). It is constituted of 80% pebbles.

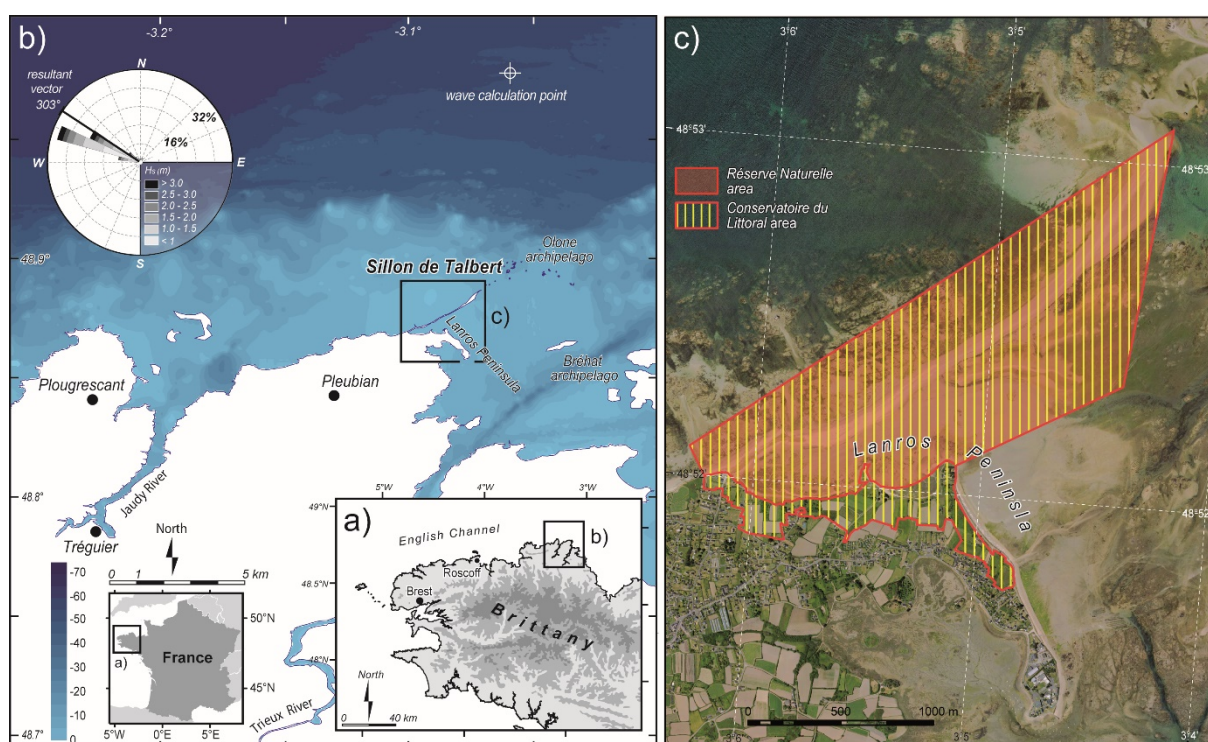


**Fig. 1.** Location map. (a) regional scale; (b) local scale. Wave rose established from the data obtained by numerical model ANEMOC over the period 1979-2002 (source: *Laboratoire National d'Hydrologie et d'Environnement, LNHE-EDF Chatou, and CEREMA-Brest*) at the calculation point 3°12.66' W, 48°56.28' N; (c) protected areas.

The studied area is located in a macrotidal to megatidal context with a maximum tidal range of 10.95 m (SHOM, 2016). The most frequent swells come from the WNW with a resultant vector around 303°. Consequently the waves break with a slight angle according to the coastline orientation ( $\approx 67^\circ$ ). This non-parallel swash alignment ( $\alpha > 0$ ) generates a longshore drift oriented to the NE. Modal heights ( $H_{sig}$ ) of deep sea waves are between 1 m and 1.5 m and modal periods ( $T_{pic}$ ) are between 9 and 10 seconds. During storms, wave heights can reach 9 m and periods of 20 seconds. In these conditions, Sillon de Talbert shelters the archipelago of Bréhat archipelago situated further to the SE, and prevents flooding of the low-lying coastal zone of the Lanros peninsula (Fig. 1).

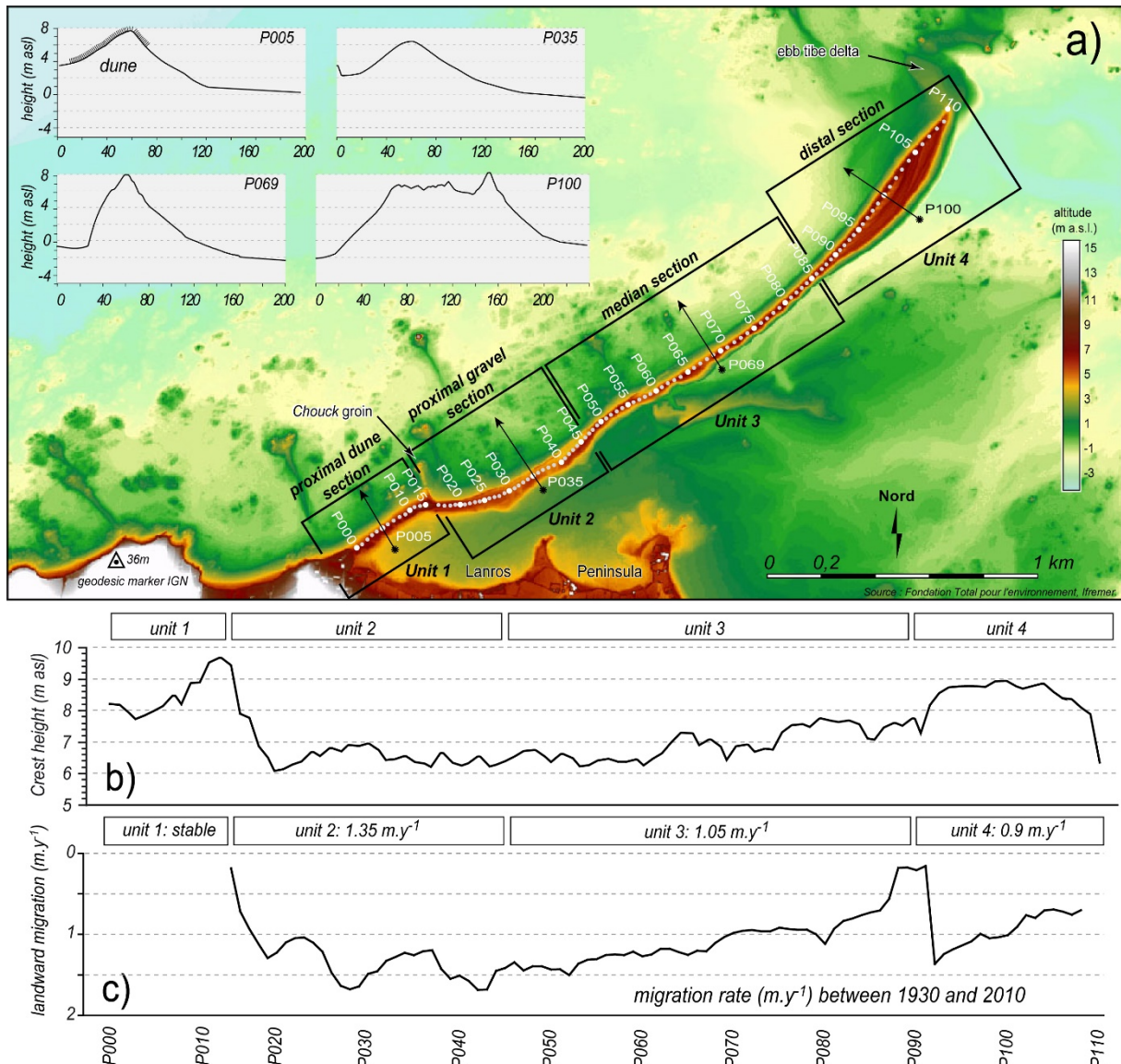


**Fig. 2.** Longshore morphological variation of the spit (a); crest height (b); landward spit displacement in  $m.y^{-1}$  (c) (from Stephan et al., 2012, modified)

Historic maps show that until the end of the 17<sup>th</sup> century, the Sillon de Talbert was connected to the islets of the Olone archipelago located on the NE (Figure 1). Its dislocation occurred in the early 18<sup>th</sup> century (Stephan et al., 2012) and is attributed to the extreme storm of 26 November 1703 which was one of the most violent events recorded over the last centuries along the South England and the Northwest French coasts (Lamb and Frydendahl, 2005). The old maps dated from this period indicated the opening of a large breach on the North-Eastern section of the original barrier which gave rise to a 3.2 km long gravel spit. This shift from anchored barrier to spit initiated a slight cannibalization process which increased throughout the 19<sup>th</sup> and 20<sup>th</sup> centuries due to the sediment depletion. To this longshore dynamic was added the cross-shore dynamic since the landward displacement of the spit by rollover was facilitated by the disconnection. Since 1770, the rate of spit retreat has been estimated at 1  $m.yr^{-1}$  (Pinot, 1994). More recently, Stephan et al. (2012) have shown that the average of the landward migration rate for the entire spit reached 1.1  $m.yr^{-1}$  between 1930 and 2010 (Fig. 2c). During the same time period, the longshore sediment transport through



cannibalization from the proximal to the distal section was evaluated at  $1.4 \text{ m}^3.\text{m}.\text{yr}^{-1}$  (Stephan et al., 2010). As indicated earlier, between the mid-70's and the beginning of the 80's, several coastal defense structures such as the 200 m long rip-rap and the Chouck groin (Fig. 3a), and the 1400 m long rip-rap were installed on the proximal and the median sections respectively, to prevent the spit barrier retreat (Pinot, 1994; Stephan et al., 2012). Because of their inefficiency, and the change in coastal management strategy when the Sillon de Talbert became the property of the "Conservatoire du Littoral" in 2001, the major part of the rip-rap of the median section was removed. The blocks of rock were crushed and the material was then deposited on the back-barrier salt-marsh at a few dozen meters from the lee edge of the back slope to form three embankments wrongly supposed to slow down the landward migration of the spit (Fig. 3a and 3b) (Stephan et al., 2012). In addition, a part of this crushed material has also been used for nourishment of some limited zones of the proximal gravel section.



**Fig. 3.** Aerial photo of the Sillon de Talbert. (a) Photo taken the 23 September 2009 (source: D. Halleux) showing the coastal defense structures on the sandy proximal section; (b) photo taken the 12 September 2007 (source: D. Halleux) showing the tip of the spit with the ridges of accretion and the ebb tide delta.

### 3. Data and methods

The monitoring is based on yearly topo-morphological measurements. It started in October 2002 and is still ongoing. Therefore, this paper presents a data set acquired over the last 15-year period, between October 2002 and September 2017 (Table 1). Three main techniques were used to collect the data set. An airborne Lidar was utilized in October 2002 with an altimetric accuracy of  $\pm 10 \text{ cm}$  (Boersma and Hoenderkamp, 2003). From the Lidar

raw data, a 3D digital elevation map (DEM) was computed using a kriging interpolation model to produce a regular 1-m grid. The computation of a 1-metre square gridding implies at least a minimum of 2.3 to 3.5 points per mesh size (Levoy et al., 2013). This condition is largely reached in this case because of the high density of points that were measured, reaching about 3 per m<sup>2</sup>.

In addition, 16 campaigns of DGPS (Differential Global Positioning System) topographic measurements were realized between 2003 and 2017, which represent more than 1 survey per year (Table 1). DGPS surveys were made during the autumn spring-tide period (generally in September or October), using RTK (Real Time Kinematics) mode. Each DGPS measurement was calibrated using the geodesic marker from the French datum and the geodesic network provided by the IGN (*Institut Géographique National*) located on the study area (Fig. 2). For each campaign's measurements, the position of the control points was measured and the margin of error for the three dimensions (x, y and z) was calculated using standard deviation. The estimated margin of error reached respectively +/-5 to 7 cm in x, y and +/- 2 cm in z. These values were used to calculate margin of error associated with the sediment budget calculation. In each survey, the space between measurements was not rigid but dependent on topography. The 10 m to 20 m interval was used in flat smooth topography, but was reduced to less than 0.5 m to 0.2 m where the topography was very rough. Surfer 9.0 software was used to import and process the (x, y, z) data. The generation of a 3D digital elevation map (DEM) was the basis for subsequent interpretation and analysis. The kriging interpolation approach supporting breaklines was adopted to generate regular 1-m grids.

Finally, two campaigns of UAV (Unmanned Aerial Vehicle) flights such as drones were conducted in 2016 (Table 1). On April 2016, the UAV flights were only used to generate an orthorectified image. On October 2016, the flights were coupled with Structure from Motion (SfM) photogrammetry to carry out the topographic survey of the studied site. During each campaign, 6 to 7 UAV flights were needed to cover the whole surface of the studied area. The survey was performed using an electric hexacopter UAV called "DRELIO" (Jaud et al., 2016), based on a multi-rotor platform DS6 (Fig. 4a). The DS6 is equipped for nadir photography with a reflex camera Nikon D800 with a focal length of 35 mm. The flight control is run by the DJI® software iOSD and was based on a preliminary defined flight plan. The flight altitude was around 115 m, which leads to a spatial resolution of 1.7 cm. The camera was setup to acquire RAW images every 10 seconds allowing a quasi-systematic image side lap higher than 60% for an optimized SfM photogrammetric process. During each aerial survey, ground control points (GCPs) were surveyed using DGPS measurements in Real Time Kinematics (RTK) mode. The SfM photogrammetric process was performed using Agisoft® Photoscan Professional software. We chose this user-friendly commercial software for its ease of use and the quality of data produced (Jaud et al., 2016). For each aerial survey, a set of about 250 to 300 images were processed separately. An additional DSM at a resolution of 1 m were produced for the 2016 UAV surveys to be compared to the Lidar and DGPS DEMs.

Date	Technology	material used	source or organism	Horizontal accuracy	Vertical accuracy	Area covered (km <sup>2</sup> )	Number of topographic data acquired on the field	Number of topographic data used to generate Grid	interpolation method	Grid resolution	Coordonnate system
22 September to 8 October 2002	Lidar airborne		IFREMER	±0.5 m	±0.1 m	3,49	638 976	638 976	kriging	1x1m	EPSG: 2154 - RGF93
15 to16 June 2003	DGPS survey	Trimble 5700-5800	Private consultancy	±0.05 m	±0.05 m	0,27	4 544	123 135	kriging with breaklines	1x1m	EPSG: 27572
18 to19 September 2005	DGPS survey	Trimble 5700-5800	Private consultancy	±0.05 m	±0.05 m	0,34	2 869	121 186	kriging with breaklines	1x1m	EPSG: 27572
29 April to 2 May 2006	DGPS survey	Trimble 5700-5800	LETG-UMR 6554 CNRS	±0.07 m	±0.03 m	0,32	4 732	122 978	kriging with breaklines	1x1m	EPSG: 2154 - RGF93
24 to 27 September 2007	DGPS survey	Trimble 5700-5800	LETG-UMR 6554 CNRS	±0.07 m	±0.03 m	0,33	9 808	128 023	kriging with breaklines	1x1m	EPSG: 2154 - RGF93
19 March 2008	DGPS survey	Trimble 5700-5800	LETG-UMR 6554 CNRS	±0.07 m	±0.03 m	*	659	no grid	-	-	-
15 to 20 September 2008	DGPS survey	Trimble 5700-5800	LETG-UMR 6554 CNRS	±0.07 m	±0.03 m	0,34	11 731	129 243	kriging with breaklines	1x1m	EPSG: 2154 - RGF93
16 to 18 September 2009	DGPS survey	Trimble 5700-5800	LETG-UMR 6554 CNRS	±0.07 m	±0.03 m	0,27	13 704	131 013	kriging with breaklines	1x1m	EPSG: 2154 - RGF93
29 to 30 April 2010	DGPS survey	Trimble 5700-5800	LETG-UMR 6554 CNRS	±0.07 m	±0.03 m	0,19	11 801	129 349	kriging with breaklines	1x1m	EPSG: 2154 - RGF93
20 to 24 September 2010	DGPS survey	Trimble 5700-5800	LETG-UMR 6554 CNRS	±0.07 m	±0.03 m	0,30	17 685	134 855	kriging with breaklines	1x1m	EPSG: 2154 - RGF93
13 to 16 September 2011	DGPS survey	Trimble 5700-5800	LETG-UMR 6554 CNRS	±0.07 m	±0.03 m	0,34	17 795	135 013	kriging with breaklines	1x1m	EPSG: 2154 - RGF93
17 to 19 September 2012	DGPS survey	Trimble 5700-5800	LETG-UMR 6554 CNRS	±0.07 m	±0.03 m	0,34	14 962	132 304	kriging with breaklines	1x1m	EPSG: 2154 - RGF93
3 to 6 September 2013	DGPS survey	Trimble 5700-5800	LETG-UMR 6554 CNRS	±0.07 m	±0.03 m	0,36	15 618	132 960	kriging with breaklines	1x1m	EPSG: 2154 - RGF93
4 to 7 March 2014	DGPS survey	Trimble 5700-5800	LETG-UMR 6554 CNRS	±0.07 m	±0.03 m	0,42	17 925	133 653	kriging with breaklines	1x1m	EPSG: 2154 - RGF93
9 to 11 September 2014	DGPS survey	TopCon Hyper V	LETG-UMR 6554 CNRS	±0.07 m	±0.03 m	0,36	19 456	135 421	kriging with breaklines	1x1m	EPSG: 2154 - RGF93
28 September to 1 October 2015	DGPS survey	TopCon Hyper V	LETG-UMR 6554 CNRS	±0.07 m	±0.03 m	0,33	30 888	146 154	kriging with breaklines	1x1m	EPSG: 2154 - RGF93
5 to 8 April 2016	UAV flights	DRELIQ exaocopter	LETG-UMR 6554 CNRS	±0.1 m	±0.1 m	*	> 10 <sup>4</sup>	no grid	-	-	-
17 to 20 October 2016	UAV flights	DRELIQ exaocopter	LETG-UMR 6554 CNRS	±0.1 m	±0.1 m	0,34	> 10 <sup>4</sup>	> 10 <sup>4</sup>	Nearest Neighbour	0.1x0.1m	EPSG: 2154 - RGF93
4 to 7 September 2017	DGPS survey	TopCon Hyper V	LETG-UMR 6554 CNRS	±0.07 m	±0.03 m	0,33	14 773	131 942	kriging with breaklines	1x1m	EPSG: 2154 - RGF93

Table 1. Inventory of the topo-morphological surveys achieved between 2002 and 2017.

Lidar topographic data of 2002 for the fixed surrounding foreshore and coastal areas were used for the calculation of each DEM to improve the 3D visualisation. Calculation of the sediment budget was achieved for each survey from the interpolated surface by calculating the volumetric difference between two surfaces based on grid subtraction. DEM of Differences (DoD) were performed following the method implemented by [Wheaton et al. \(2009\)](#). Net change ( $\Delta z_{net}$ ) and the absolute change ( $\Delta z_{max}$ ) were generated from the interpolated surface plots with the vertical change (m) presented for each 1 m<sup>2</sup> grid cell. Volume calculation was focusing on (i) the material deposited on the crest by overtopping, (ii) sediment accumulated on the back-barrier slope by overwash process, (iii) sediment deposited in the distal section due to the longshore sediment transfert (Figure 4c). Each DEM was also sliced into 110 cross-shore transects along which two main morphological indicators such as crest lowering/accretion ( $\Delta z_{crest}$ ) and (ii) landward spit migration ( $\Delta_{retreat}$ ) were measured (Fig. 4d). The quantification of the spit retreat was achieved using the landward limit of the rear as best shoreline limit between the gravel sediments of the spit barrier and the mud of the back-barrier low-lying zone (Fig. 4b).

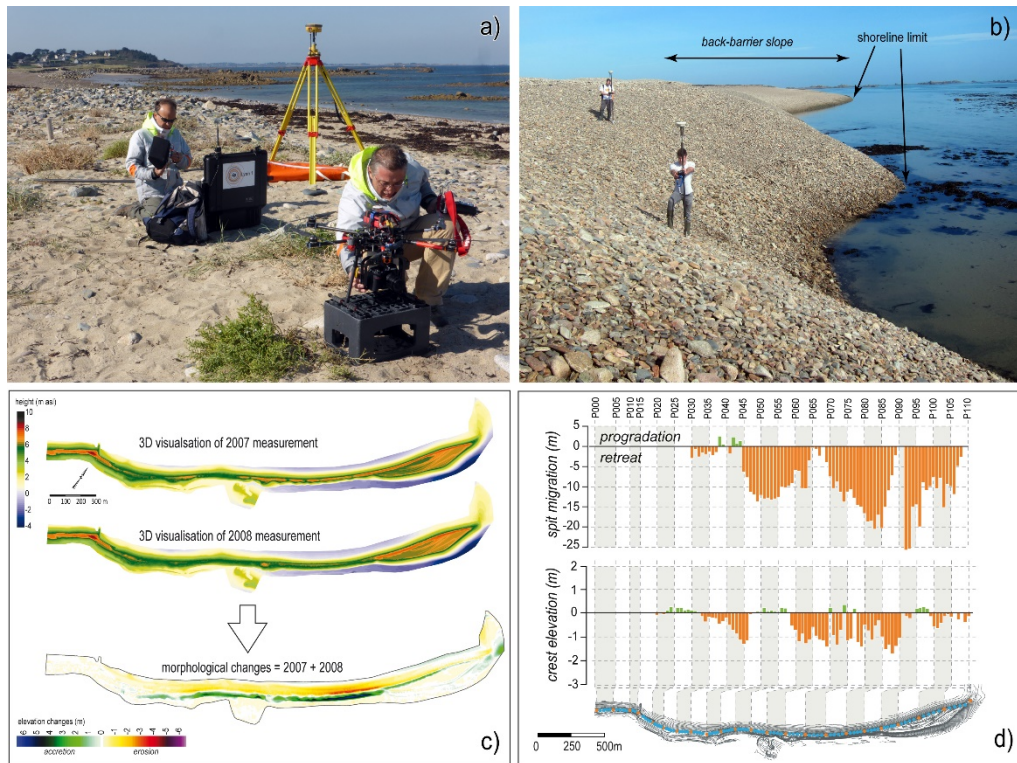


**Fig. 4.** Techniques of topo-morphological measurements. (a) Deployment of the electric hexacopter UAV called “DRELIO”. (b) DGPS measurements and back-barrier slope of the spit showing the limit between gravel and mud sediment. This limit is used as a proxy for shoreline analysis. (c) Analysis of morphological changes and calculation of sediment budget given in elevation changes. (d) Calculation of landward spit displacement and the lowering/elevation of the crest.

## 4. Results

### 4.1. Sediment budget

Fig. 5 shows DEMs and DoDs produced over the entire study period 2002-2017. In most cases, the erosion is affecting the seaward beach face while the deposition concerns the back-barrier, reflecting the rollover process of the spit barrier. This was especially the case between 2007 and 2008, and between 2013 and 2014. These two examples illustrate the morph-sedimentary changes generated by the storm of March 10, 2008 (Stephan et al., 2010), and by the cluster of storms during the winter of 2013-2014 (Blaise et al., 2015), respectively. Important topographic variations are also observed on the ebb tide delta situated on the tip of the spit. These topo-morphological changes are related to longshore sediment transport from the proximal to the distal section and the sediment removal caused by the interaction of incident waves and the ebb tidal currents on this zone. During storm events, sediments are moved from the front to the center of the deltaic lobe while under fair-weather conditions, the sediments are transferred to the deltaic front under the predominant influence of ebb tidal currents. The tip of the spit is also affected by significant morphological changes and sediment transfers either to the northwest or to the southeast. The back-barrier beach face of the distal section shows a significant accretion over the entire survey period 2002-2017, especially in the upper part of the beach profile where new ridges were formed. Most DoDs indicate an alternation of erosion and accretion sub-cells along this back-barrier section. This morphology reflects the longshore sediment transfer oriented to the SE due to wave diffraction on the tip of the spit. This pattern of back-barrier sediment transfer is also observed on the median section, especially during periods without storm activity. The sub-cells of longshore deposition and erosion alternate over short distances generating

rhythmic morphology of low-amplitude on the back-barrier beach slope. This morphology reflects a south-eastward sediment transfer involving a few hundred cubic meters.

During the whole study period 2002-2017, the morphological changes are characterized by a strong temporal variability. Some periods are characterized by high amplitude topographic variations affecting the whole spit. The analysis of the sediment budget involved in the overwash processes shows that the landward sediment transfers are very episodic. However, two periods of massive washover, i.e. September 2007–September 2008 and September 2013–March 2014, that reached about 120,000 m<sup>3</sup> and 175,000 m<sup>3</sup> respectively, are identified (Fig. 6a). Between 2002 and 2017, the total overwashing induced a net volume of back-barrier deposition reaching about +370,000 m<sup>3</sup> (Fig. 7). On the proximal section, the washover fans due to these cross-shore sediment transfers, have gradually covered the two first embankments. Therefore, the net sediment budget related to rollover process represents about 30% of the global sediment volume of the gravel barrier spit. However, the periods of overwash are most often followed by recovery periods during which the morphology of the spit is stable and overtopping processes are dominant. These recovery processes occurred under fair climate conditions, following periods of intense storm activity, i.e. between 2009-2012 or 2015 (Fig. 6b).

Suivi topo-morphologique du Sillon de Talbert – Pleubian – Période 2016-2017

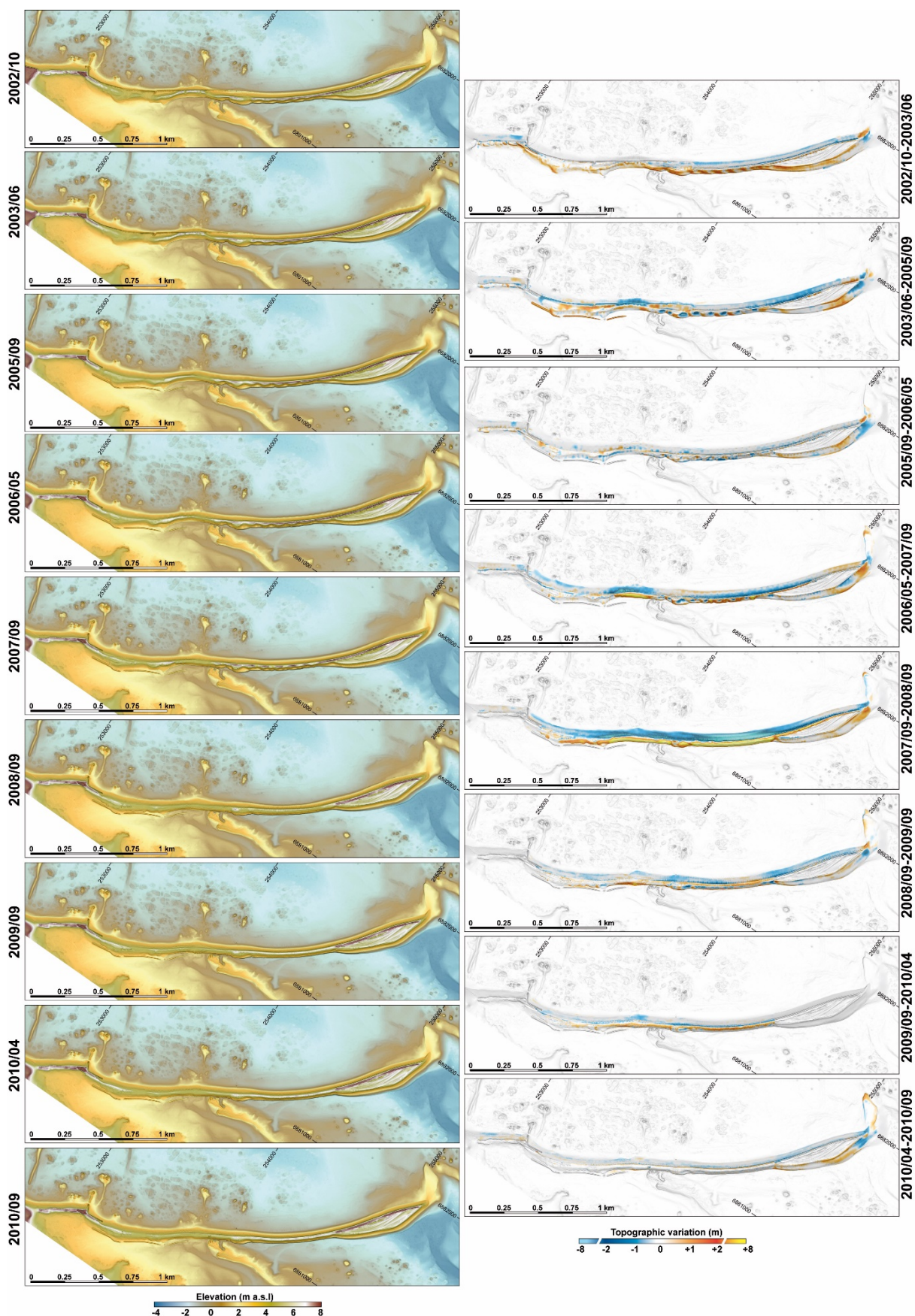
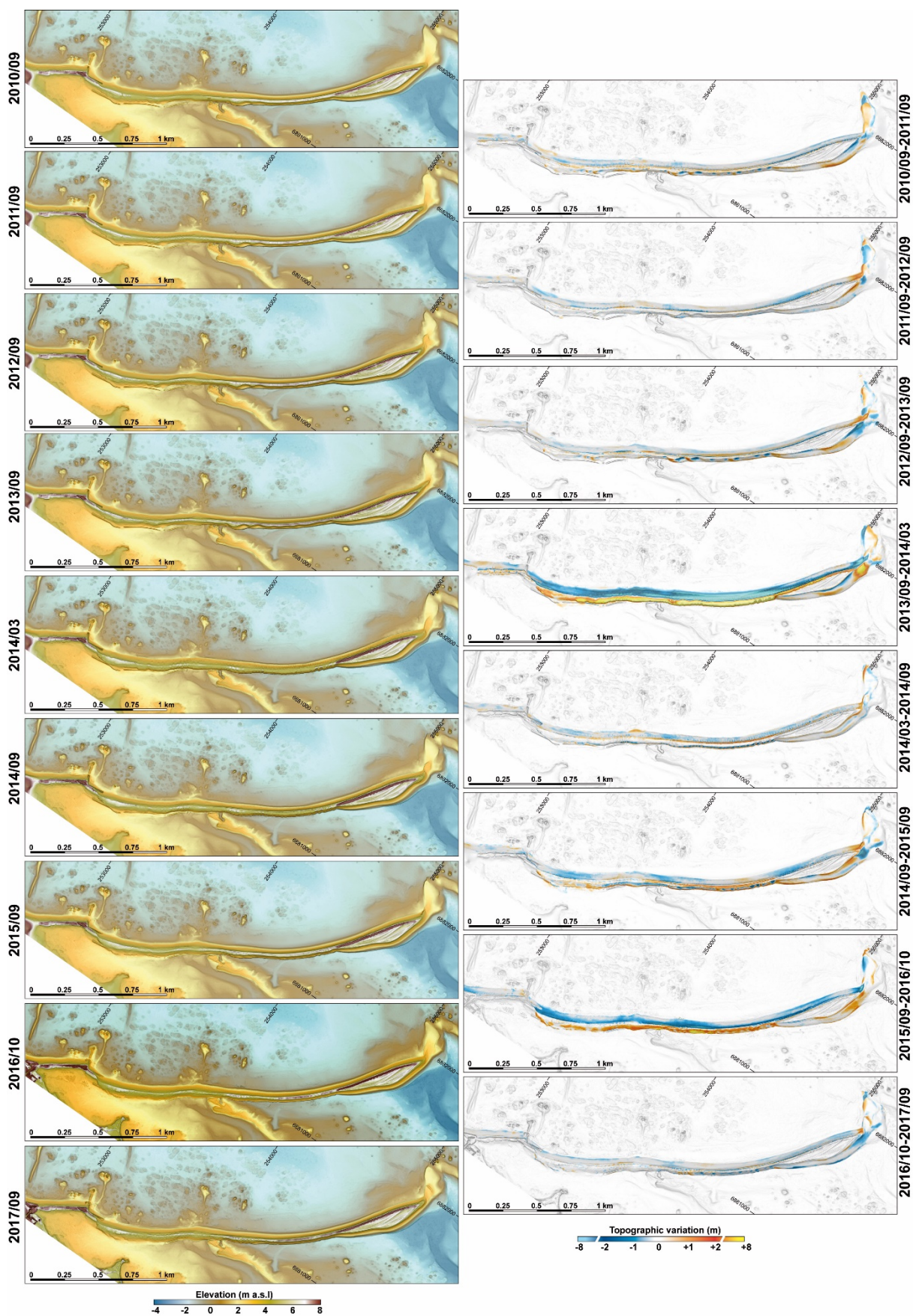


Fig. 5. DEMs of the Sillon de Talbert gravel spit and DoD produced between 2002 and 2017.

*Suivi topo-morphologique du Sillon de Talbert – Pleubian – Période 2016-2017*



**Fig. 5 (continued).** DEMs of the Sillon de Talbert gravel spit and DoD produced between 2002 and 2017.

As shown on Fig. 7, over the whole surveyed period the seaward beach face erosion is estimated to  $-411,000 \pm 26,000 \text{ m}^3$ , while the back-barrier deposition is about  $+420,000 \pm 20,000 \text{ m}^3$ . The net balance between the sediment volumes eroded and deposited indicates a relative conservation of the whole sediment volume of the spit. The sediment volume accumulated on the back-barrier spit ( $+370,000 \text{ m}^3$ ) corresponds in around 90% to overwashed material involved in the rollover process. Based on the calculation of the sediment volume accumulated on the back-barrier of the tip of the spit (i.e. distal section), the northeastern longshore sediment diffracted on the tip of the spit is estimated at  $50,000 \pm 4,400 \text{ m}^3$  (Fig. 7). These longshore transfers are relatively constant over time and reach about  $3,200 \text{ m}^3/\text{year}$  on average (Fig. 6c and 7). This longshore sediment transport is realized through a cannibalization process added to the barrier rollover.

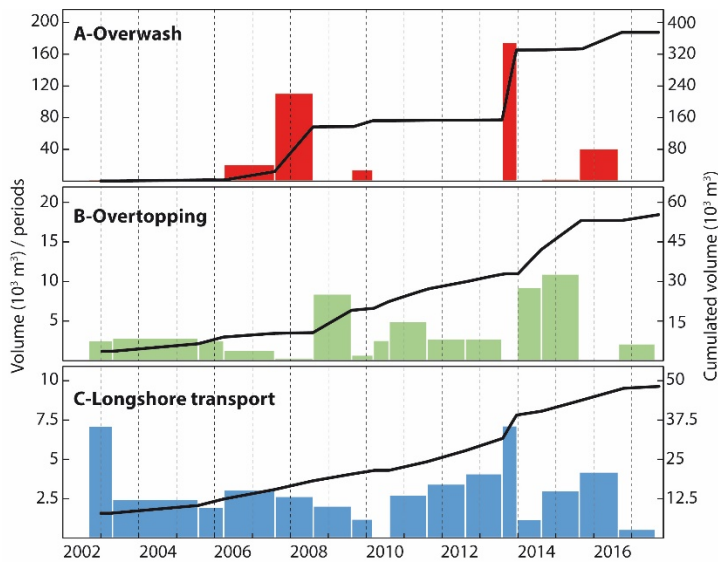


Fig. 6. Temporal variations in sediment volumes involved in overwash events (a), crest overtopping (b) and longshore transport (c).

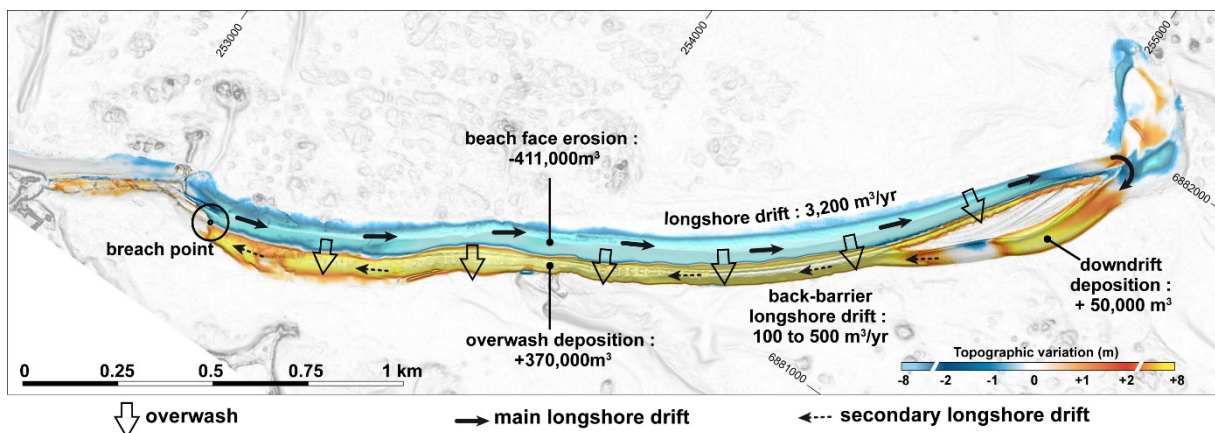


Fig. 7. Sediment budget of the Sillon de Talbert on the period 2002-2017.

#### 4.2. Spit retreat ( $\Delta_{\text{retreat}}$ )

The results of the barrier mobility show that the average of landward displacement of the spit reached about  $-31.2 \text{ m}$  between 2002 and 2017 while the maximum retreat up to  $-66.30 \text{ m}$  was recorded in the distal section along the transect P091 (Fig. 8a). The proximal gravel section (P016 to P045) retreated by an average of about  $-18.87 \text{ m}$  over the entire period, with a maximum of about  $-$



53.37 m. This retreat due to rollover process led to washover fans which have today completely covered the embankments #1 and #2 (Fig. 9b). Similarly, the median (P046 to P085) and distal (P086 to P110) sections experienced a significant average landward migration of -39.2 m and -28.89 m, respectively. The maximum and minimum retreating values for the median section were -63.13 (P052) m and -18.60 m (P067) respectively, and -66.30 m (P091) and 0 m (P108-109) respectively for the distal section (Fig. 8a). Regarding the annual frequencies (Fig. 8c), two major events inducing landward displacement are clearly identified; the year 2008 due to the impact of the storm of March 10, 2008, and the year 2014, related to the cluster of storms of the winter 2013-2014. During these two events, the maximum landward migration reached -22.70 m (on the distal section) and -30.10 m (on the proximal gravel section), respectively; during these two events, the average retreat for the whole spit was -6.45 m and -11.14 m, respectively.

#### **4.3. Crest evolution ( $\Delta_{z_{crest}}$ )**

During the surveyed period 2002-2017, the crest recorded high variations in elevation (Fig. 8b). The largest crest lowering of about -1.03 m was recorded on the median section (P068), it reached -0.95 m (P108) and -0.60 m (P018) on the distal and proximal sections, respectively. Conversely, the crest elevation reached +1.66 m (P037), +1.02 m (P067), and +1.01 m (P097) on the proximal, medial, and distal sections, respectively. With a mean crest elevation of +11.82 m and a standard deviation of 0.49 m, the median section recorded the most significant changes from 2002 to 2017. The annual frequencies also indicated the very significant morphogenic impact of the storm of March 10, 2008, and the cluster of storms during the winter 2013-2014 (Fig. 8d). During these two events, the maximum lowering of the crest occurred on the median section, and reached -2.44 m and -1.79 m, respectively. However, after each of these episodes, recovery processes due to overtopping resulted in crest elevation reaching its pre-storm height.

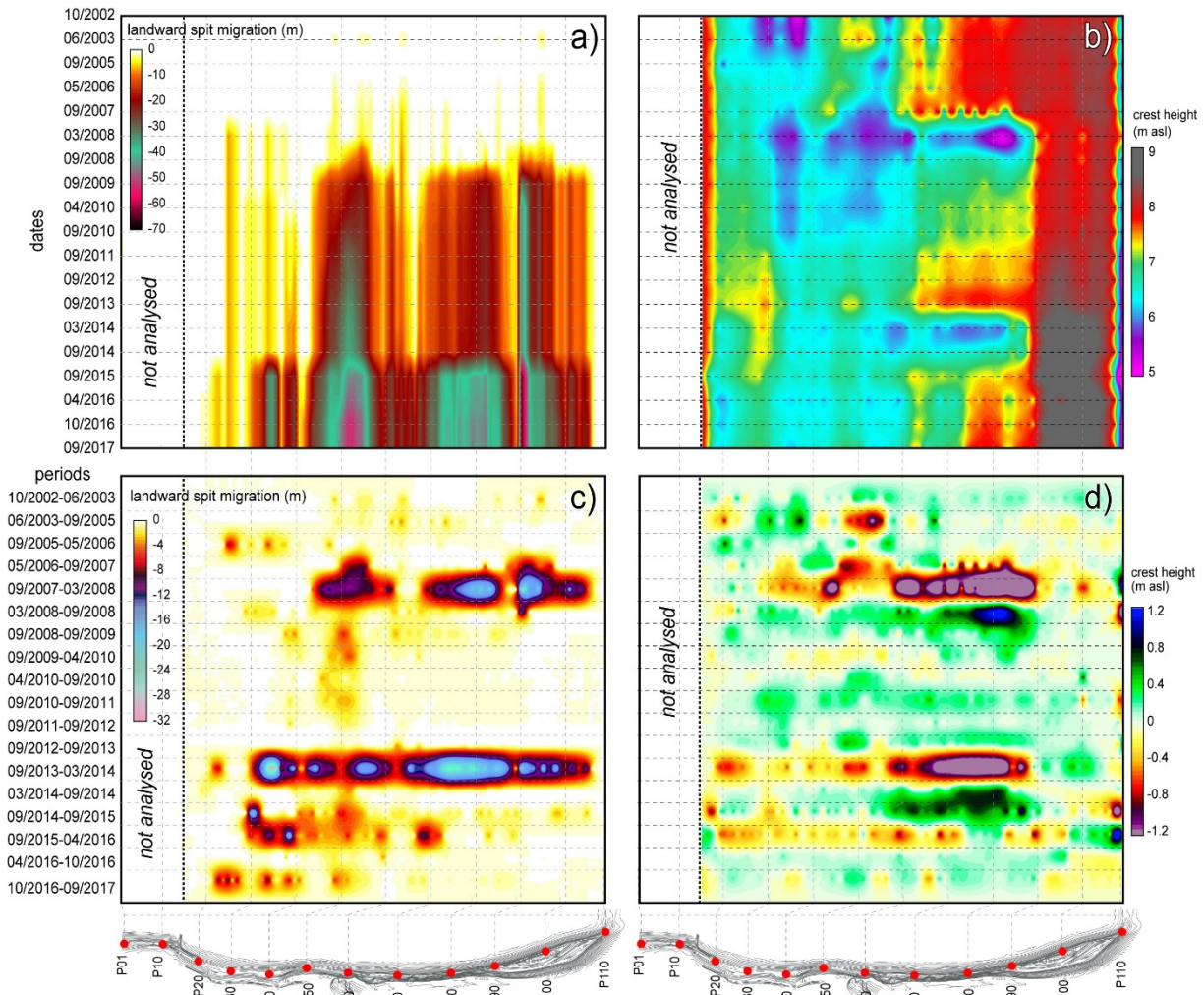


**Fig. 8.** Morphological changes of the spit between 2002 and 2017. Landward spit migration ( $\Delta z_{\text{retreat}}$ ) in cumulated frequencies (a) and annual frequencies (b), crest lowering/accretion ( $\Delta z_{\text{crest}}$ ) in cumulated frequencies (c) and annual frequencies (d).

## 5. Threat of spit breaching on the “wasp waist” section

The retreat of the Sillon de Talbert gravel spit during the whole survey period has led to the weakening of a small section located downdrift of the *Chouck* groin (Fig. 9a and 9b). This section which has been called in French “*la taille de guêpe*” that can be translated by the “wasp waist”, is characterized by a significant barrier lowering and narrowing. Currently, the spit is threatening to breach in the proximal section where a 150 long remaining rip-rap is supposed to prevent the spit retreat. However, as shown in Fig. 9c and 9d, during the last decade this rip-rap was totally disconnected from the base of the barrier due to the retreat of the shoreline; today, it no longer plays the role of protection against erosion.



**Fig. 9.** Morphological changes of the proximal section situated on both sides of the *Chouck* groin over the whole survey period: (a) 29/03/2002 (source: IGN - CA00S01232\_FR5415\_250\_1181); (b) 19/10/2016. Shoreline retreat of the gravel proximal section between 2005 (c) and 2014 (d). This section called “wasp waist” is nowadays threatening to break.

The “wasp waist” section is composed by a mixture of sand and gravel, essentially on the beach face while the sand fraction is dominant on the top barrier. In 2002, the top barrier consisted of a 30 m wide low-elevated sandy dune connected to the rip-rap at its base (Fig. 9a and 9c). Over the last 15 years, the shoreline, identified by the highest astronomical tide level, has been in constant retreat (Fig. 10a). The barrier, lying against the rip-rap along its entire length in 2005, was disconnected from it on 60% of its length in 2016 and the shoreline experienced a retreat of a dozen meters. The calculation of sediment budget between 2002 and 2017 shows that this zone has lost about  $-11,000 \pm 2,500 \text{ m}^3$  (Fig. 10b). However, the interannual evolution of the sediment budget indicated three distinct phases (Fig. 10c). The first phase from 2002 to 2006 shows an increase of the sediment budget related to anthropogenic forcing (Fig. 10c). As mentioned above, some nourishments on localized areas (i.e. throats) were realized with gravel derived from rip-rap crushing. The second phase from

2006 to 2013 is characterized by a stable sediment budget, even if the shoreline has retreated (Fig. 10c). In fact, the seaward beach-face erosion was compensated by a back-barrier slope deposition due to the rollover process. After 2013, the sediment budget is characterized by a net loss. The most significant erosion occurred during the winter 2013-2014 (Fig. 10d) with a shoreline retreat of about – 10 m to –15 m. During this winter the dune was totally flooded by wave runup. Several hundred cubic meters of sediments were overwashed from the seaward beach-face to the back-barrier, reducing the width of the vegetated dune to a few meters. The last significant shoreline retreat occurred in 2016 during the storm Imogen in February 2016 (Fig. 10e). In October 2016, as shown by the aerial photo (Fig. 9b), the dune vegetation has vanished, and a series of washover fans are visible in the back-barrier. In 2017, the limit of highest astronomical tide level indicates an incipient breach (Fig. 10a). This topo-morphological evolution is the result of the both longshore (i.e. cannibalization) and cross-shore (i.e. rollover) processes, exacerbated by the interruption of the up-drift sediment inputs by the *Chouck* groin. Thus, the opening of a breach is dramatically expected soon.

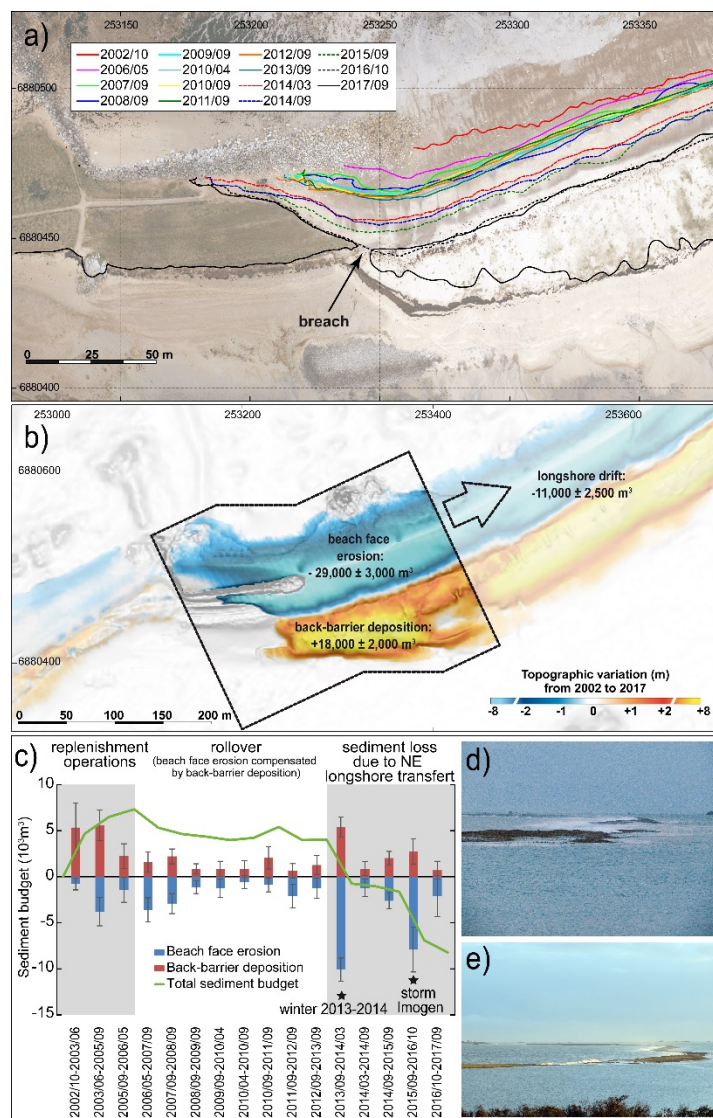


**Fig. 10.** Shoreline changes between 2002 and 2017 indicated by the highest astronomical tide (HAT) level extracted from DEMs produced from 2002 to 2017 (a). Calculation of the sediment budget in the zone of the “wasp waist” between October 2002 and September 2017 (b). Interannual evolution of the sediment budget in the zone of the “wasp waist” between October 2002 and September 2017 (c). Overwash episode during the storm Dirk of the winter 2013-2014 (photo: Jacky Laveaud, 04/01/2014) (d). Overwash episode during the storm Imogen of February 2016 (photo: Julien Houron, 11/02/2016) (e).

## 6. Discussion

### 6.1. The barrier response to storm (resilience trajectory)

Sediment budget calculation of the Sillon de Talbert between 2002 and 2017 indicated a dominant cross-shore sediment transfer driven by overwash processes especially during storms. The total volume of sediment transferred on the back-barrier by washovers was estimated around 370,000 m<sup>3</sup> that corresponds to about 30% of the whole spit sediment volume. An extrapolation of this result indicates that at current rates, the time required for a complete remobilization of the material forming the gravel spit barrier is approximately 50 years. Although this period of time seems very short today, the overall morphology of the barrier has been preserved and no breach has formed. This highlights the strong resilience of the barrier. Orford (2011), and Orford and Anthony (2011) defined such resilience in the context of gravel barriers, as a measure of barrier morpho-sedimentary adjustment by which any outcomes of positive feedback mechanisms imposed by extreme forcing (state change), are subsequently reworked by the reintroduction of negative feedback mechanisms that rebuild the barrier towards the initial state. These authors estimate the barrier height ( $B_h$ ) and the width of the crest ( $B_w$ ) are the two critical elements for all barrier survival and indexes the overall stability of the crest. The barrier resilience can be considered in terms of the time pathway (resilience trajectory) of  $B_h$  and  $B_w$  variations from pre-event to some point post-event when the crest re-built to some form of geomorphological stability. As proposed by Orford and Anthony (2011),  $B_w$  can be define as the ridge width which is calculated at the HWST level. In our study, the profile analyses conducted between 2002 and 2017 indicates significant variations in the elevation of the crest along the barrier. Fig. 13a shows the variations in the crest elevation ( $B_h$ ) and the ridge width ( $B_w$ ) on profiles P030 (proximal gravel section) and P081 (median gravel section). Two different resilience trajectories clearly appear regarding the beach crest rebuilding (after a storm events). Along the profile P030, the barrier experienced a significant lowering during the storm Johanna of 10 March 2008. Despite limited erosion during the following storm events and an overall trend to the crestal rebuilding on the period 2008-2017, the barrier hasn't recovered the initial elevation. During the surveyed period, the width of the barrier decreased gradually from around 60 m in 2002 to 50 m in 2017 (Fig. 13a). In the proximal gravelly section, the crest is topped by small-size embryonic sand dunes and the rebuilding activity after a storm overwashing event is determined by the aeolian sand supplies and the interaction with the vegetation cover. Along the profile P081, the crest elevation was highly impacted by the storm of 10 March 2008 and during the winter 2013-2014 which caused a lowering of -2.44 m and -1.73 m, respectively. After these storm events, the elevation of the ridge was below the highest astronomical tide (HAT) level and became highly sensitive potential further flooding events. Although this situation was critical and could represent a tipping point towards a barrier breaching, the post-storm rebuilding of the ridge occurred during the following months. The topo-morphological survey indicates that the prestorm elevation of the crest has recovered by three to four years after, in the absence of a new intense overwash event. This particular resilience trajectory, characterized by a high rebuilding capacity is typical of gravel-dominated coastal systems where overtopping acts as a negative feedback process. The evolution of the  $B_w$  parameter along the profile P081 shows an increase of the ridge width during the stormy period of the winter 2013-2014 (Fig. 13a). As previously

suspected by Orford and Anthony (2011), these morphological changes may have acted as a brake to over-crest flow, favoring the post-storm crestal deposition.

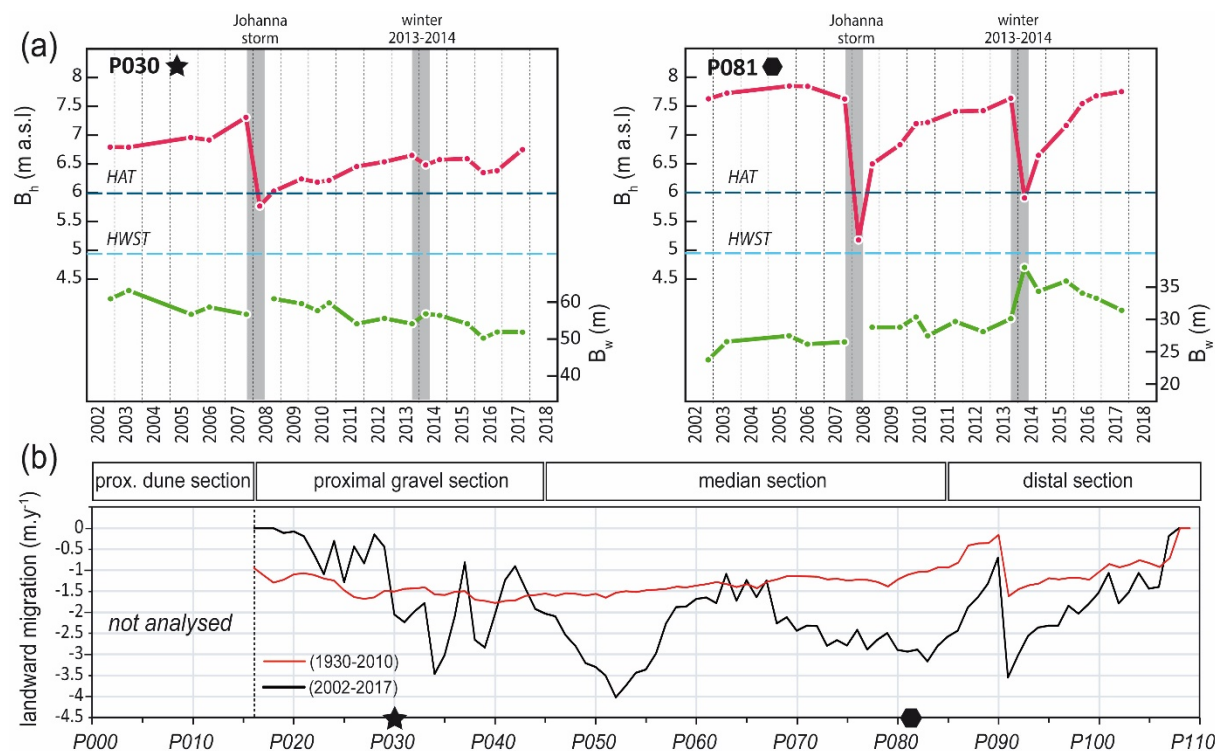


**Fig. 11.** Topo-morphological changes of the Sillon de Talbert between October 2002 and September 2017. (a) Crest height ( $B_h$ ) and ridge width ( $B_w$ ) variations on the proximal gravel section (profile P030) and on the median section (profile P081). Landward spit migration rates calculated for the three gravel proximal, median and distal sections for both periods 1930-2010 (from Stéphan et al., 2012) and 2002-2017.

## 6.2. Acceleration of the barrier retreat

The Sillon de Talbert experienced important landward migration rates over the last 15 years, with maximum values reaching  $-3$  to  $-4 m \cdot y^{-1}$  depending on the morphological units (Fig. 11b). By comparison, the migration rates calculated by Stephan et al. (2012) over the last decades (1930-2010) indicated maximum values around  $-1.5 m \cdot y^{-1}$ . While the global volume of the spit and the barrier inertia stayed relatively constant over the last decades, such differences in the values of migration rates raises the question of an enhanced storminess or a wave climate change (or variability) in Northern Brittany during recent years. Fig. 12 shows the mean migration rates of the Sillon de Talbert calculated by linear regressions –taking into account the average values calculated for all 110 transects– over the last 80 years (period 1930-2010) and over the last 15 years (period 2002-2017). Data indicates that the rate of the barrier retreat is twice as great as prior to 2002 when the monitoring began ( $-2 m \cdot y^{-1}$  vs  $-1.2 m \cdot y^{-1}$ ). We observe that the construction of the artificial embankments on the back-barrier which were supposed to slow-down the retreat did not work. This acceleration is mainly related to the significant impact of the March 10, 2008, Johanna storm and the cluster of storms during the winter 2013-2014. However, note that the period between 1961 and 1966 also was characterized by an acceleration of barrier retreat just as significant. As indicated by several authors (Cariolet, 2011, Stephan et al., 2012, Stephan et al., 2018), this period was characterized by two severe storm episodes combined with high spring tide: that of April 5, 1962 and January 17 to 20, 1965. This suggests that variations in the migration rates over the multi-decade time scale may be simply due to

the impact of some severe storm events over a short time, without significant change of the long term tendency.

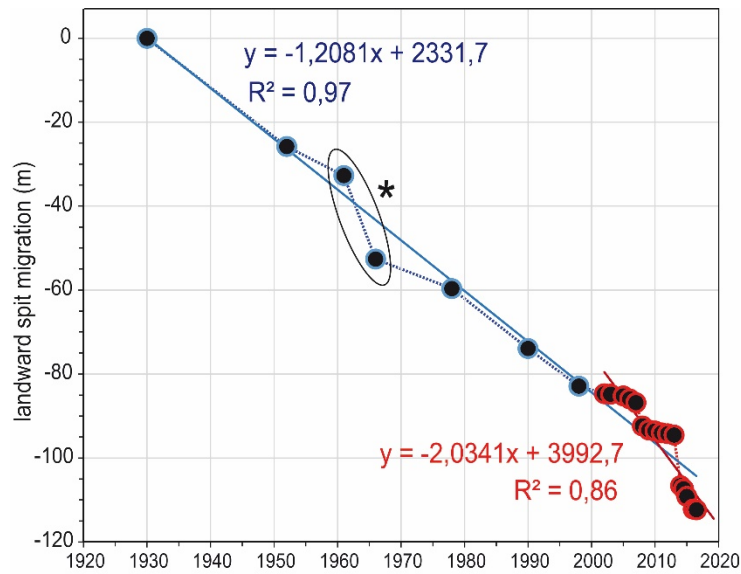


**Fig. 12.** Landward spit migration rates calculated for the three proximal, median and distal morphological units for both periods 1930-2010 (from Stéphan et al., 2012) and 2002-2016. The asterisk (\*) indicates the acceleration of spit retreat between 1961 and 1966.

The northeastward longshore sediment transport over the whole survey period has led to a sediment accumulation on the distal section reaching about 50,000 m<sup>3</sup>. Based on the observation of the old maps of the early 18<sup>th</sup>, [Stephan et al. \(2012\)](#) have shown that the geometric plan-view morphology of the Sillon de Talbert adopted a more drift-aligned orientation while it was still connected to the Olone archipelago ([Fig. 3a](#)). The transformation of the barrier into a spit barrier due to the disconnection of the tip triggered a northeastward longshore sediment transport and a significant accretion of the distal part of the spit. [Stephan et al. \(2015\)](#) pointed out the depletion of gravel supply from the offshore zone along the Brittany coast. Nowadays, most of the gravel barriers are fed with coarse material mainly provided by the erosion of soft cliffs composed by periglacial deposits. However, erosion of soft cliffs appears too slow to deliver significant volumes of coarse sediments into the coastal sediment cells. This situation is responsible for the retreat of most of the gravel spits in Brittany over the last decades ([Stephan, 2011](#); [Stephan et al., 2015](#)). Because the soft cliffs, situated up-drift the Sillon de Talbert, are now stabilized by the vegetation and/or high perched on the bedrock at their base, the erosion process has decreased and the up-drift sediment supply has been considerably reduced. Therefore, the longshore sediment transport from the proximal to the distal section of the Sillon de Talbert is realized through cannibalization processes that increased over the last centuries/decades. Nevertheless, many studies have shown that the final stage of the cannibalization process is the dislocation of the barrier through the breach opening in their proximal part ([Kidson, 1964](#); [Aubrey and Gains, 1982](#); [Carter and Orford, 1991](#); [Orford et al., 1991, 1996, 2002](#); [Jolicoeur et al., 2010](#); [Bujalesky and Bonorino, 2015](#); [Sabatier and Anthony, 2015](#)). Thus, the morphological changes recorded

between 2002 and 2017 in the proximal section – “wasp waist” beach– suggest the opening of a breach into the spit barrier in the next few years.

### 6.3. Coastal management strategies

Two strategies in terms of coastal erosion management, particularly in the area of the “wasp waist”, are noted according to the interests of the “Conservatoire du Littoral”, as owner of the land, and the municipality of Pleubian which has to manage the coastal risks on its communal land.

As indicated earlier, since the Sillon de Talbert became the property of the Conservatoire du Littoral, a new coastal management based on the “principle of accompaniment of the natural evolution driven by natural forcing” was adopted. In addition, the topo-morphological survey over the last 15 years indicated that the remaining rip-rap was ineffective to protect the “wasp waist” sector against erosion. Even more, solutions based on the use of hard coastal structures such as the *Chouck* groin accelerated the erosion process by blocking the longshore sediment transfer from upstream to downstream drifting. Therefore, the management strategy promoted by the “*Conservatoire du Littoral*” is to remove the rip-rap and the *Chouck* groin in order to restore the longshore sediment transport from the sandy to the gravel beach of the proximal section (Fig. 13). As shown on the Figure 13a, the sandy beach/dune section situated up-drift of the *Chouck* groin extends 140 m wide towards the sea due to the blocking of sediments by the groin. Similarly, the difference in beach height on either side of the groin is about 2 m. Thus, the removing of the *Chouck* groin would have the immediate impact of generating a massive sediment transfer to restore the sediment budget balance between the two sections (Fig. 13b). However, an intense erosion of the up-drift sandy beach/dune due to the regularization of the shoreline process would be expected immediately in the months following the removal of the groin. This rapid evolution could lead to the opening of a large breach as shown in the scenarios (c) and (d) of the Fig. 13. Most likely, the opening of a breach –and its rapid expansion over time– would constitute a threat in the coastal flooding area for the Lanros Peninsula – and the houses standing there– because the Sillon de Talbert would no longer play the role of natural protection against waves and/or surges.

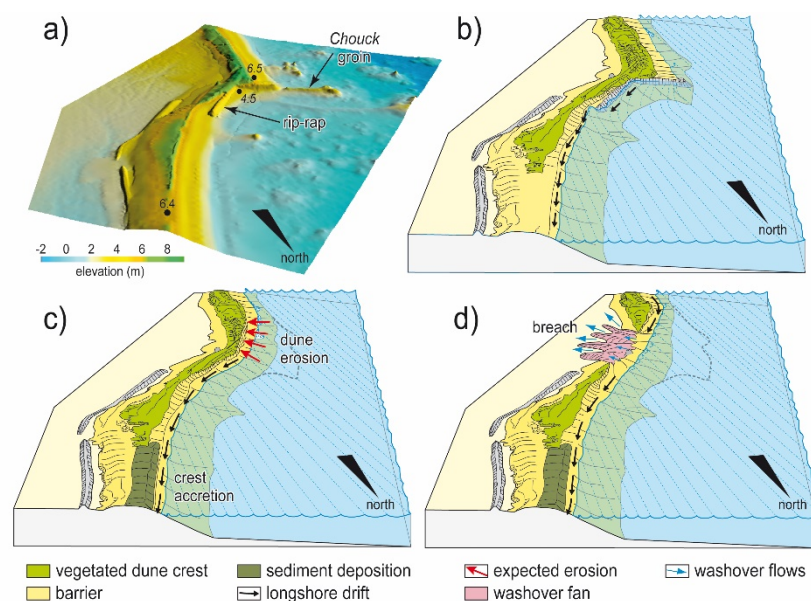


**Fig. 13:** Morphological evolution of the beaches situated upstream and downstream of the *Chouck* groin after it has been removed. (a) Current topo-morphological context. (b) Massive longshore sediment transfer from the upstream to the



downstream beaches. (c) Erosion due to the regularization process of the shoreline by waves. (d) Opening of a breach due to the shoreline retreat.

The second option promoted by the municipality of Pleubian is based on the fact that if a breach occurs in the proximal section of the spit, as mentioned above, the Sillon de Talbert would no longer play the role of protecting the Lanros Peninsula against coastal flooding. This situation would increase the coastal risk in this area where houses are located very close to the shoreline and at a very low elevation (Figure 3b). Therefore, a “soft” solution would be the replenishment of the threatened zone of the “wasp waist” beach with gravel sediments extracted from the zones where the sediment budget is in excess. This option as a soft coastal defense management against erosion would be an intermediate solution in terms of interventionist engineering strategy. Indeed, because of the widely held perception that hard stabilization is destructive to recreational beaches, beach replenishment is often viewed as a better solution to the erosion problem (Pilkey and Clayton, 1989; French, 2001; Pupier-Dauche, 2002). Along the Channel coast, several programs of sediment replenishment were implemented over the last two decades to ensure the stability of some gravel barriers and spits, such as the Hurst Castle Spit in Christchurch Bay (Hampshire, UK) (Nicholls and Webber, 1987a, 1987b), or the Hourdel gravel spit in Cayeux-sur-Mer (Somme, France) (Dolique 1998; Dolique and Anthony 1999). In both cases, the option of beach replenishment has replaced a previous coastal management strategy based on hard defense structures. On the Sillon de Talbert, the volumetric requirements to fill the “wasp waist” area have been estimated to around 14,300 m<sup>3</sup>. This volume takes into account the reshaping of the plan-view morphological profile of the shoreline (Fig. 14a). However, the U.S. East coast barrier islands beach replenishment experience showed that when post-replenishment loss rates are compared to pre-replenishment (*i.e.* natural) loss rates, the post-replenishment rates are found to be one and a half to twelve times greater (Leonard et al., 1990). In the Netherlands the volume of fill sediments exceeded the volumetric requirements by 20%; some like Verhagen (1996) even considered that a 40% overrun should be considered in order to mitigate the effects of beach profile readjustment and the lateral sediment losses. These experiences suggest that future beach design models should not base volumetric predictions on the assumption that annual replenishment volume requirements will be equal to historical average annual erosional losses on the natural beach. Theoretically, the success of beach replenishment is also largely dependent on the grain size of fill material which must closely matches the native material, or even be slightly coarser (Berg and Duane 1968; Leonard et al., 1990; Newman 1976). However, storm activity in terms of frequency and intensity, is the most important factor in determining beach durability after nourishment. Some other parameters, such as beach length, grain size, shoreface slope, shelf width and method of fill emplacement may also play a role in beach replenished lifetime (Dixon and Pilkey, 1989; Leonard et al., 1990). Leonard et al. (1990) indicated that replenished beaches north of Florida generally have lifetimes of fewer than 5 years. Therefore, this 5-year period corresponds to a reasonable time interval for renewal beach nourishment. According to these findings, the volumetric requirements to fill the “wasp waist” area should be increased by 20 to 40%, e.g. 17,200 m<sup>3</sup> to 20,000 m<sup>3</sup>.

Concerning the source sites for required materials, an option is to extract gravel sediment accumulated on the ebb delta northeast of the spit (Fig. 14b). Between 2002 and 2017, the total volume of sediment of this area remained stable, indicating that it does not contribute to the global sediment changes of the Sillon de Talbert. The calculation of the available stocks has been estimated to 6,600 m<sup>3</sup> to 15,000 m<sup>3</sup> depending to the depth extraction (Fig. 14c and 14d). In addition, 3,900 m<sup>3</sup> may be used with the crushing of the rip-rap which would be removed (Fig 14a). A total volume of 10,500

m<sup>3</sup> to 18,900 m<sup>3</sup> is therefore available to fill the “wasp waist” zone. Furthermore, some other sources of gravel accumulations for extraction exist on the rocky platform.

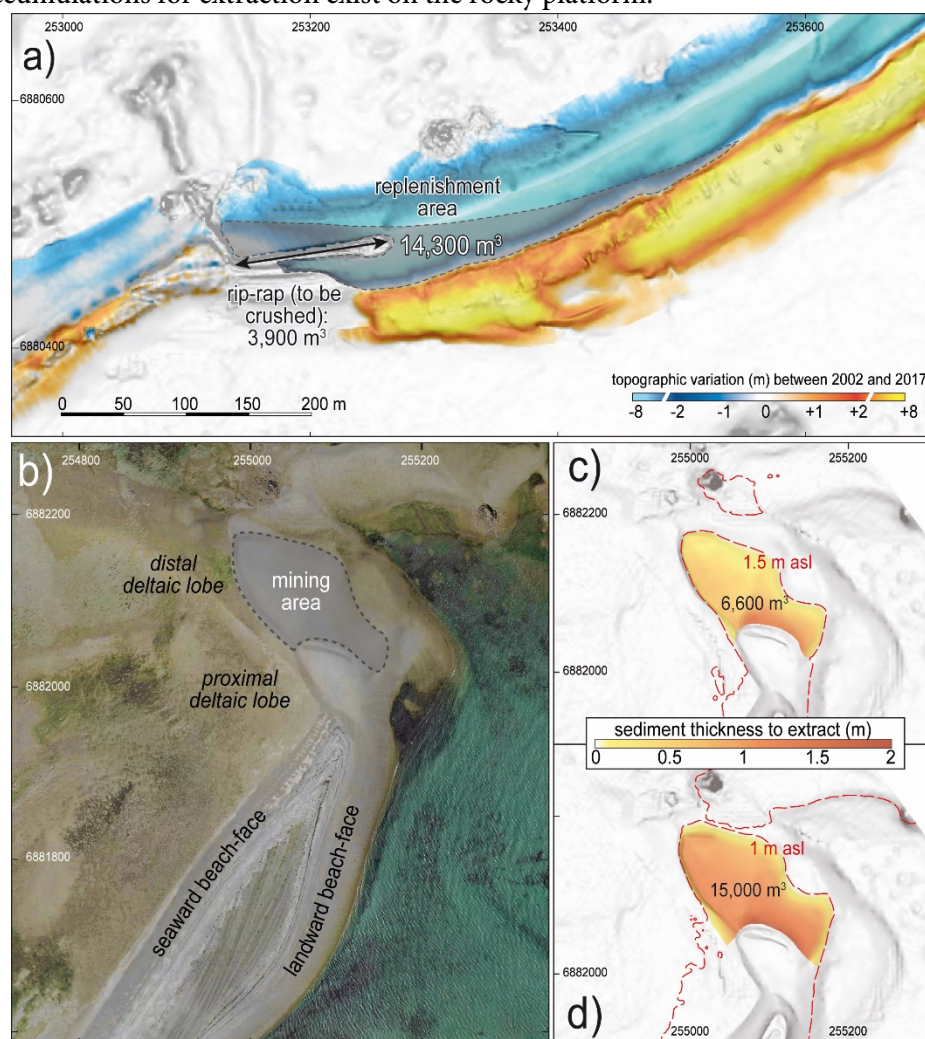


**Fig. 14:** Potential source of sediment on the ebb delta in the north of the Sillon de Talbert (a). Sediment thickness above 1.5 m asl and corresponding available volume (b). Sediment thickness above 1.5 m asl and corresponding available volume (c). Replenishment area mapped on the DoD 2002-2017 (d).

## Conclusion

The topo-morphological monitoring of the Sillon de Talbert undertaken between 2002 and 2017 significantly improves the understanding of the morphological and sedimentary behaving of the gravel spits. The conceptual approaches describing the longshore and cross-shore dynamics are fully illustrated by the annual measurements made over the last 15 years. Based on the DEMs production and comparison, this monitoring allowed accurate calculation of sediment volumes involved in the morphological changes which are summarized as follow:

1- The spit exhibits a rapid landward migration, with maximum average rate of 4 m.y<sup>-1</sup> during years characterized by significant storm events combined with high spring tides (e.g., 10 March 2008 storm of Johanna, or the cluster of storms during the winter 2013-2014). This

landward displacement increased during the last fifteen years to almost twice the rate during the 20<sup>th</sup> century (2 m.yr<sup>-1</sup> vs 1.2 m.yr<sup>-1</sup>).

2- The sediment budget calculation shows that cross-shore transfers are dominant and represented a total volume of 370,000 m<sup>3</sup> during the survey period. Considering this volume, we assume that a period of 50 years is required to remobilize the total volume of the Sillon de Tabert (i.e., 1.2 10<sup>6</sup> m<sup>3</sup>). However, despite this high long-term mobility, the barrier experienced no breaching; this indicates strong resilience processes resulting in very effective post-storm morphological adjustments, especially through crest rebuilding processes. However, the actual evolution of the proximal gravel section of the spit (e.g., “wasp waist” section) indicates that these resilience processes are no longer acting.

3- The longshore sediment transfer through cannibalization phenomenon was estimated at about 50,000 m<sup>3</sup> from 2002 to 2017. This evolution is also responsible for weakening the proximal gravel section that suffers from a lack of sediment. The depletion of sediment supply in this zone is directly due to the *Chouck* groin which interrupts the up-drift longshore transport, and confirms the negative effects of such structures on beach morphosedimentary functioning.

4- This survey provided relevant scientific expertise to support a coherent coastal erosion management strategy. If the chosen option is moving towards beach replenishment, the data collected allows for a more precise estimate of the volumetric requirements (i.e., between 17,200 m<sup>3</sup> to 20,000 m<sup>3</sup>), and defines suitable areas to extract gravels for beach nourishment. However, the actual coastal management policy adopted by the “*Conservatoire du Littoral*”, and the authority of the Brittany Region, is mainly based on the new option strategy in terms of shoreline management promoted by the French ministry of “*Ministère de la transition écologique et solidaire*”. This strategy called “*stratégie nationale de gestion intégrée du trait de côte*” is actually encouraging the withdrawal of stakes, such as houses, instead of protecting the shoreline against erosion by the use of engineering approaches (e.i. hard coastal structures or beach replenishment). In view of the dynamics described here, this latter approach is probably the safer and more economic solution in the long term.

### **Acknowledgements**

This work was supported by the municipality of Pleubian and the Conservatoire du littoral. We are grateful to the staff of these two partners who provided technical assistance in the field and many observations during the surveyed period. It was also supported by the French “Institut National des Sciences de l’Univers” (INSU) under-program, SNO-DYNALIT. Authors are grateful to William Neal, Julian Orford and the anonymous reviewer for their constructive comments.

### **References**

Aubrey, D.G., Gains, A.G., 1982. Rapid formation and degradation of barrier spits in areas with low rates of littoral drift. *Mar. Geol.* 49, 257–278.

Benavente, J., del Río, L., Plomaritis, T.A., Menapace, W., 2013. Impact of coastal storms in a sandy barrier (Sancti Petri, Spain). *J. Coast. Res.* 65 (SI), 666–671.

Berg, D.W., Duane, D.B., 1968. Effect of particle size and distribution on stability of artificially filled beach. *Presque Isle Peninsular, Pennsylvania. Proceedings of the 11<sup>th</sup> Conference on Great Lakes research*, 161–78.

Blaise, E., Suanez, S., Stephan, P., Fichaut, B., David, L., Cuq, V., Autret, R., Houron, J., Rouan, M., Floc'h, F., Arduin, F., Cancouët, R., Davidson, R., Costa, S., Delacourt, C., 2015. Bilan des tempêtes de l'hiver 2013-2014 sur la dynamique de recul du trait de côte en Bretagne. *Géomorphologie : relief, processus, environnement* 21, 267–294.

Boersma, S.M, Hoenderkamp, K. 2003. Tregor, final report IFREMER, Amsterdam.

Bujalesky, G.G., Bonorino, G.G. 2015. El Paramo Transgressive Gravel Spit, Tierra del Fuego, Argentina, in: Randazzo, N., Jackson, D., Cooper A., (Eds.), *Sand and Gravel Spits*, Springer Ed., Coastal Research Library 12, Springer, pp. 37–50.

Buscombe, D., Masselink, G., 2006. Concepts in gravel beach dynamics, *Earth-Science Rev.* 79, 33-52.

Butt, T., Russell, P., 2000. Hydrodynamics and cross-shore sediment transport in the swash-zone of natural beaches: a review. *J. Coast. Res.* 16, 2, 255–268.

Cariolet, J.M., 2011. Quantification du runup sur une plage macrotidale à partir des conditions morphologiques et hydrodynamiques. *Geomorphologie Relief, Processus, Environment* 1, 95–108.

Carter, R.W.G., Orford, J.D., 1991. The sedimentary organisation and behaviour of drift-aligned gravel barriers, in: Kraus, N.C., Gingerich, K.J., Kriebel, D.L., (Eds), *Coastal Sediments '91: proceedings of a special conference on quantitative approaches to coastal processes*, Seattle, Washington, June 25–27, vol 1, American Society of Civil Engineers, New York, pp. 934–948.

Carter, R.W.G., Orford, J.D., 1984. Coarse clastic barrier beaches: a discussion of the distinctive dynamic and morphosedimentary characteristics. *Mar. Geol.* 60 (1–4), 377–389.

Carter, R.W.G., Orford, J.D., 1993. The morphodynamics of coarse clastic beaches and barriers: a short and long-term perspective. *J. Coast. Res.* 15 (SI), 158–179.

Davies, J.L., 1972. *Geographical variation in coastal development*, Oliver and Boyd, Edinburgh.

Dixon, K.-W., Pilkey, O.-H. 1989. Beach replenishment on the U.S. Gulf of Mexico shoreline. Proceedings of Coastal Zone'89 Conference, New York, 2007–2020.

Dolique, F., 1998. Dynamique morphosédimentaire et aménagement induits du littoral picard au sud de la baie de Somme. PhD thesis, Université du Littoral Côte d'Opale, Dunkerque.

Dolique, F., Anthony, E.J., 1999. Influence à moyen terme (10-100 ans) d'un estran sableux macrotidal sur la stabilité d'un cordon de galets : la flèche de Cayeux (Picardie, France). *Géomorphologie : relief, processus, environnement*, 1, 23–38.

Donnelly, C., Kraus, N., Larson, M., 2006. State of knowledge on measurement and modeling of coastal overwash. *J. Coast. Res.* 22, 965–991.

French, P.W., 2001. Coastal defenses: processes, problems and solutions, Routledge, London.

Holman, R.A., Sallenger, A.H., 1985. Setup and swash on natural beach. *J. Geophysical Res.* 90, 945–953.

Hudson, C., Bailly, B., 2018. Delivering sustainable coasts: Monitoring the long-term stability of a breached barrier beach, Porlock Bay, Somerset, United Kingdom. *Ocean. Coast. Manag.* 152, 88–99.

Jaud, M., Passot, S., Le Bivic, R., Delacourt, C., Grandjean, P., Le Dantec, N., 2016 Assessing the Accuracy of High Resolution Digital Surface Models Computed by PhotoScan® and MicMac® in Sub-Optimal Survey Conditions. *Remote Sens.* 8, 6, 465. doi:10.3390/rs8060465

Jennings, R., Shulmeister J. 2002. A field based classification scheme for gravel beaches. *Mar. Geol.* 186, 211–228.

Jiménez, J.A., Sánchez-Arcilla, A., 2004. A long-term (decadal scale) evolution model for microtidal barrier systems. *Coast. Eng.* 51, 749–764.

Jolicoeur, S., Giangioppi, M., Bérubé, D., 2010. Réponse de la flèche littorale de Bouctouche (Nouveau-Brunswick, Canada) à la hausse du niveau marin relatif et aux tempêtes entre 1944 et 2000. *Géomorphologie : relief, processus, environnement* 1, 91–108.

Kidson, C., 1964. Dawlish Warren, Devon: Late stages in sand spit evolution. Proceedings of the Geologists' Association, 75 (2), 167–184.

Lamb, H.H., Frydendahl, K., 2005. Historic storms of the North Sea, British Isles and Northwest Europe, Cambridge University Press, Cambridge.

Leonard, L.-A., Clayton, T., Pilkey, O.-H. 1990. An analysis of replenished beach design parameters on U.S. east coast barrier islands. *J. Coast. Res.* 6 (1), 15–36.

Levoy F., Anthony E.J., Monfort O., Robin N., Bretel P., 2013. Formation and migration of transverse bars along a tidal sandy coast deduced from multi-temporal Lidar datasets. *Mar. Geol.* 342, 39–52.

Masselink, G., Li, L. 2001. The role of swash infiltration in determining the beachface gradient: a numerical study. *Mar. Geol.* 176, 139–156.

McCall R., Masselink G., Poate T., Roelvink D., Almeida L.P., 2015. Modelling storm morphodynamics of gravel beaches during storms with XBeach-G. *Coast. Eng.* 103, 52–66.

Newman, D.-E., 1976. Beach replenishment: sea defenses and a review of the artificial beach replenishment. *Proceedings of the Institution of Civil Engineers* 6 (60), 45–60.

Nicholls, R.J., Webber, N.B., 1987a. The past, present and future evolution of Hurst Castle Spit, Hampshire. *Progress in Oceanography* 18, 119–137.

Nicholls, R.J., Webber, N.B., 1987b. Coastal erosion in the eastern half of Christchurch Bay, in: Culshaw, M.G., F.G. Bell, J.C. Cripps, M. O’Hara (Eds), *Planning and Engineering Geology*, Geological Society, London, Engineering Geology Special Publication, 4, pp. 549–554.

Orford, J.D., Carter, R.W.G., 1982. Crestal overtop and washover sedimentation on a fringing sandy gravel barrier coast, Carnsore Point, Southeast Ireland. *J. Sedimentary Res.* 52 (1), 265–278. Doi: 10.1306/212F7F2C-2B24-11D7-8648000102C1865D

Orford, J.D., Carter, R.W.G., Forbes, D.L., 1991. Gravel barrier migration and sea level rise: some observations from Story Head, Nova Scotia, Canada. *J. Coast. Res.* 7, 477–488.

Orford, J.D., Carter, R.W.G., 1995. Examination of mesoscale forcing of a swash-aligned, gravel barrier from Nova Scotia. *Mar. Geol.* 126, 201–211.

Orford, J.D., Carter, R.W.G., Jennings, S.C., Hinton, A.C., 1995. Processes and timescales by which a coastal gravel-dominated barrier responds geomorphologically to sea-level rise: Story head barrier, Nova Scotia. *Mar. Geol.* 20, 21–37. Doi: 10.1002/esp.3290200104

Orford, J.D., Carter R.W.G., Jennings, C.S., 1996. Control domains and morphological phases in gravel-dominated barriers of Nova Scotia. *J. Coast. Res.* 12(3), 589–604.

Orford, J.D., Forbes, D.L., Jennings, S.C., 2002. Organisational controls, typologies and time scales of paraglacial gravel-dominated coastal systems. *Mar. Geol.* 48, 51–85. Doi: 10.1016/S0169-555X(02)00175-7

Orford, J.D., 2011. Gravel-Dominated coastal barrier reorganisation variability as a function of coastal susceptibility and barrier resilience. *Coastal Sediments '11*, 1257–1270.

Orford, J.D., Anthony, E.J., 2011. Extreme events and the morphodynamics of gravel-dominated coastal barriers: strengthening uncertain ground. *Mar. Geol.* 290, 41–45. Doi: 10.1016/j.margeo.2011.10.005

Pilkey, O.H., Clayton, T.D. 1989. Summary of beach replenishment experience on U.S. East coast barrier islands. *J. Coast. Res.* 5, 147–159.

Pinot, J-P., 1994. Fixer le plan ou gérer le profil : l'exemple du Sillon du Talbert. *Cahiers Nantais*, 41–42, 307-316.

Pupier-Dauchez, S. 2002. Le rechargement sédimentaire : De la défense des côtes à l'aménagement du littoral (Analyse des pratiques sur la côte Atlantique française), PhD thesis, Université de Bretagne Occidentale, Brest.

Sabatier, F., Anthony, E., 2015. The Sand Spits of the Rhône River Delta: Formation, Dynamics, Sediment Budgets and Management, in: Randazzo, N., Jackson, D., Cooper A., (Eds.), *Sand and Gravel Spits*, Springer Ed., Coastal Research Library 12, Springer, pp. 259–274.

Sallenger, A.H., 2000. Storm Impact Scale for Barrier Islands. *J. Coast. Res.*, 16, 3, 890–895.

SHOM, 2016. Références altimétriques maritimes – Ports de France métropolitaine et d'outre-mer. Côtes du zéro hydrographique et niveaux caractéristiques de la marée. Service Hydrographique et Océanographique de la Marine, Brest.

Stephan P., Suanez S., Fichaut B. (2010). Franchissement et recul des cordons de galets par rollover, impact de la tempête du 10 mars 2008 dans l'évolution récente du Sillon de Talbert (Côte d'Armor, Bretagne). *Noréis*, 215, 52–58.

Stephan, P., 2011. Quelques données nouvelles sur la mobilité récente et le bilan sédimentaire des flèches de galets de Bretagne. *Géomorphologie : Relief. Processus. Environnement*, 2, 205–232.

Stephan, P., Suanez, S., Fichaut, B., 2012. Long-term morphodynamic evolution of the Sillon de Talbert gravel barrier spit, Brittany, France. *Shore & Beach*, 80 (1), 19–36.

Stephan, P., Suanez, S., Fichaut, B., 2015. Long-, Mid- and Short-Term Evolution of Coastal Gravel Spits of Brittany, France, in: Randazzo, N., Jackson, D., Cooper A., (Eds.), *Sand and Gravel Spits*, Springer Ed., Coastal Research Library 12, Springer, pp. 275–288.

Stephan, P., Dodet, G., Tardieu, I., Suanez, S., David, L., 2018. Dynamique pluri-décennale du trait de côte en lien avec les variations des forçages météo-océaniques au nord de la Bretagne (baie de Goulven, France). *Géomorphologie : relief, processus, environnement*, in press. DOI: 10.4000/geomorphologie.11908

Stockdon, H.F., Sallenger, A.H., Holman, R.A., Howd, P.A., 2007. A simple model for the spatially-variable coastal response to hurricanes. *Mar. Geol.* 238, 1–20.

Tillmann, T., Wunderlich, J., 2013. Barrier rollover and spit accretion due to the combined action of storm surge induced washover events and progradation: Insights from ground-penetrating radar surveys and sedimentological data. *J. Coast. Res.* 65 (SI), 600–605. Doi: 10.2112/SI65-102.1

Verhagen, H.-J., 1996. Analysis of beach nourishment schemes. *J. Coast. Res.* 12, 179–185.

Wheaton, J.M., Brasington, J., Darby, S.E., Sear, D.A., 2009. Accounting for uncertainty in DEMs from repeat topographic surveys: improved sediment budgets. *Earth Surf. Process. Landforms* 35, 136–156.

Zenkovitch, V.P., 1967. *Processes of coastal development*, Oliver and Boyd, Edinburgh.